Morphodynamic adaptation timescales of the Guyana mangrove-mudflat system
Are coastlines shaped by migrating mudbanks more resilient against sea level rise?

Best, Üwe S.N.; Legay, Alexandre; Reyns, Johan; van der Wegen, Mick

DOI
10.1002/esp.70135

Publication date
2025

Document Version
Final published version

Published in
Earth Surface Processes and Landforms

Citation (APA)
Best, Ü. S. N., Legay, A., Reyns, J., & van der Wegen, M. (2025). Morphodynamic adaptation timescales of the Guyana mangrove-mudflat system: Are coastlines shaped by migrating mudbanks more resilient against sea level rise? *Earth Surface Processes and Landforms*, *50*(10), Article e70135. https://doi.org/10.1002/esp.70135

Received: 1 January 2025 | Revised: 6 June 2025 | Accepted: 22 July 2025

DOI: 10.1002/esp.70135

RESEARCH ARTICLE

ESPL WILEY

Morphodynamic adaptation timescales of the Guyana mangrove-mudflat system: Are coastlines shaped by migrating mudbanks more resilient against sea level rise?

Üwe S. N. Best[1,2] | Alexandre Legay[3] | Johan Reyns[1,2,4] | Mick van der Wegen[1,2,4]

[1]Department of Hydraulic Engineering, Delft University of Technology, Delft, The Netherlands

[2]Department of Coastal & Urban Risk & Resilience, IHE Delft Institute for Water Education, Delft, The Netherlands

[3]Université Grenoble Alpes, The French National Centre for Scientific Research (CNRS), INRAE, IRD, Grenoble INP, IGE, Grenoble, France

[4]Department of Marine and Coastal Systems: Applied Morphodynamics, Deltares, Delft, The Netherlands

Correspondence
Üwe S. N. Best, Department of Hydraulic Engineering, Delft University of Technology, Delft, The Netherlands.
Email: u.s.n.best@tudelft.nl

Funding information
The research presented in this paper was conducted within the scope of PhD research titled "Advancing Adaptation Measures for Fringing Mangrove-Mudflat Coastlines under Climate Change Impacts: Sea Level Rise & Storms" (no. 107440 for Uwe S. N. Best). The doctoral research is financed jointly by the Lamminga Fund Foundation, Deltares and IHE Delft.

Abstract

In developing effective and resilient coastal management strategies, it is critical to consider the coastline's natural spatial and temporal variation. This is particularly relevant for Guyana's wave-exposed mud-dominated coastline, where longshore migrating subtidal mudbanks create a 30-year cycle of accretion and erosion of the coastline, driven by the presence or absence of a mudbank. These cyclic dynamics are integral to the broader coastal system, shaping the development of both the mudflat profile and the opportunistic mangrove vegetation. This study aims to enhance our understanding of the behaviour of mangrove-mudflat systems on the Guyana coast by examining: (1) intertidal sediment dynamics and vegetation dynamics on a mangrove/mudflat profile, (2) the morphodynamics associated with the cyclically varying forcing conditions and (3) the processes involved in the morphodynamic response under sea level rise. We utilized an open-source, 1D, cross-shore model (Mflat) that couples tidal flow, wave action, sediment transport and morphodynamic development to vegetation dynamics, including temporal and spatial growth of the tree population and bio-accumulation. The mudflat dynamics are highly determined by the cyclically varying sediment influx, wave height and period, whereas the mangrove vegetation tends to follow the evolution of suitable intertidal areas rather than impacting morphodynamic changes. An important finding is that the time scale of the cyclically varying boundary conditions (30 years) is much shorter than the system's characteristic morphodynamic adaptation timescale, so no formal equilibrium is reached for a given boundary condition. The cyclic mangrove-mudflat system shows considerable resilience to sea level rise due to the abundance of mud, though it gradually drowns under larger sea level rise scenarios. These insights on the survivability of these intertidal systems are relevant to many other mangrove-mudflats worldwide.

KEYWORDS
biogeomorphology, mangroves, migrating subtidal mudbanks, mud coasts, mudflats, sea level rise

1 | INTRODUCTION

The geomorphological development of coastal ecosystems, such as intertidal mudflats and mangrove fringes, is directly influenced by offshore and nearshore dynamics. These dynamics affect hydrodynamic forces, sediment supply and bed levels (Baptist, 2005; Burger, 2005) and function at varying spatial and temporal scales. Relative SLR, anthropogenic influences and hydrometeorological

forces such as storm surges and wave dynamics also play significant roles (Ellison, 2015; Gardel et al., 2011; Horstman, 2014; Mariotti & Fagherazzi, 2013; Roelvink & Reniers, 2011). For example, wave action mobilizes and transports the sediment, together with the tidal forces, along the nearshore mudflat area (Augusseau et al., 2025; Augustinus, 1978; Augustinus, 1987; de Vries et al., 2024; Winterwerp et al., 2013). These mud deposits in turn create suitable conditions for the growth of the mangroves, and together they protect vulnerable sections of the coastal hinterland.

Mangrove fringes provide extensive ecosystem services and support biological diversity, making them a crucial interface between the ocean and the coastal hinterland (Mcivor et al., 2013; Woodroffe, 1990; Zhang et al., 2012). Their role in flood protection is well documented, as mangroves reduce wave energy and flow velocities, contributing to increased stabilization and sedimentation in vegetated intertidal areas (Best et al., 2022b; Blankespoor, Dasgupta, & Lange, 2017; Horstman et al., 2018; Kobayashi, Raichle, & Asano, 1993; Lugo & Snedaker, 1974; Toorman et al., 2018; van Wesenbeeck et al., 2022; van Zelst et al., 2021). These effects are driven by the high frictional dissipation caused by the dense mangrove vegetation impeding tidal currents and waves (Burger, 2005; Horstman et al., 2018; Mazda et al., 2006; Mcivor et al., 2012). Consequently, these ecosystem services enable mangrove-mudflat environments to be effective sinks for fine sediments from rivers and coastal waters. However, their low relief makes them vulnerable to sea level rise (SLR) in the context of climate change and adaptation. This study examines the cross-shore dynamics and considerations needed to enhance the resilience of similar mangrove-mudflat coasts under SLR.

Intertidal mudflats act as nature's first line of defence against coastal storms, dissipating energy over their gentle slopes and evolving towards equilibrium states under steady conditions. Such equilibrium profiles have been modelled and shown to be resilient against short-term forces like storm waves. (Elmilady et al., 2019; Maan et al., 2015; Maan et al., 2018; van der Wegen et al., 2017; van der Wegen, Roelvink, & Jaffe, 2019). Mangroves along open coasts can influence wave dynamics and can affect the long-term development and resilience of intertidal mudflat systems (Winterwerp et al., 2013). However, whether they are simply opportunistic and depend on the physical processes or are instrumental and their biophysical processes influence the sedimentation and the developing geomorphology, continues to be explored (Swales et al., 2015; Woodroffe et al., 2016). Mangroves thrive in environments with low wave heights and high sediment concentrations but may retreat under high wave conditions and low sediment supply (Toorman et al., 2018). Their extensive root structures help trap sediments, enhancing their environment (Best, 2017; Gardel et al., 2011). However, whether these process persists on longer, decadal time scales and how they relate to the system's adaptation to SLR is still debatable (Swales et al., 2015). Understanding these processes and their timescales is crucial for implementing effective nature-based coastal protection strategies.

Migrating mudbanks are present along various extensive coastlines worldwide e.g., the Kerala coast, India (Samiksha et al., 2017), along the Yellow River delta, Bohai Sea of China (Ren & Shi, 1986), the Guiana's coastline in South America: Brazil, French Guiana, Suriname, Guyana and Venezuela (Augustinus, 2004; Best et al., 2022b; de Vries et al., 2022; Eisma & van der Marel, 1971; Wells & Coleman, 1981) and in the Florida Bay, United States (Taylor & Purkis, 2012). These mudbanks, especially those along the Guiana coast, are relatively wide with higher migration speeds and influence coastline changes. The dimensions and distinct characteristics of these areas are provided in more detail in Section 2.1. The behaviour of mudbanks has been studied extensively using conceptual models, field observations and remote sensing observations, but there are limited numerical modelling representations (Allison & Lee, 2004; Allison, Nittrouer, & Kineke, 1995; Augustinus, 2004; de Vries et al., 2022; Vantrepotte et al., 2013; Walcker et al., 2015; Wells & Coleman, 1981). Here, the dynamic equilibrium theory, i.e. when there is a net zero sediment transport, has been used to explain the evolution of the intertidal mudflat under tidal and wave drive forces across different timescales (Friedrichs, 2011; Hu et al., 2018; Roberts, Le Hir, & Whitehouse, 2000). During the 'mudbank phase', mudbanks promote the formation and expansion of intertidal convex-shaped mudflats and mangrove fringes. Conversely, in the 'interbank phase', these features erode, forming a concave-shaped profile, resulting in habitat loss (Figure 1a). The transition between these phases is gradual, with a delay in mangrove habitat loss due to continued sediment supply (Best et al., 2022b; de Vries et al., 2024). Optimal coastal management strategies involve ensuring sufficient mangrove widths and monitoring mudbank positions for proactive interventions, essential for stabilizing coastlines (Smits et al., 2022). Therefore, within this research, we use a step-by-step approach in determining the influence of each external influence (tides, waves, cyclicity of the mudbanks and sea level rise) on the development of the internal zone of Guyana.

Net accretion over long time scales, such as SLR (> 100 years), is system-dependent due to complex interacting mechanisms. Mangrove resilience depends on the balance between accretion and relative SLR, requiring an understanding of non-linear feedback among hydrodynamic conditions, sediment inputs, plant productivity and elevation changes. Increased inundation from SLR can lead to higher sedimentation and bed elevation changes in some cases, while in others, it results in losses due to species exceeding their physiological limits (Xie et al., 2022). These limits are determined by their tolerance to salinity, tidal inundation, temperature extremes and nutrient availability, with species-specific adaptations such as salt exclusion, secretion and specialized root structures enabling survival in harsh coastal environments (Adame et al., 2021; Friess et al., 2022; Winterwerp et al., 2013). Global projections indicate intermediate to high increases (~SSP 4.5, 8.5) in mean sea level from 0.5 m to 1 m in this region by 2,100 (Friess et al., 2022; IPCC, 2013; Masson-Delmotte et al., 2021; Slangen et al., 2023). Subsidence due to groundwater extraction was not relevant along this section of Guyana's coast (Dalrymple & Pulwarty, 2006; Douglas, 1995; Khan & Sturm, 1995).

1.1 | Focus of the research

This study addresses the mangrove-mudflat system coastline dynamics resulting from larger mudbank migration along the wave-exposed Guyana coastline. The purpose of this research targets the increasing complexity of the boundary conditions: (1) the morphodynamic evolution of the mangrove/mudflat system to an equilibrium state under tidal forcing, (2) the morphodynamics associated with cyclically varying forcing conditions reflecting mudbank migration and (3) the morphodynamic response to SLR.

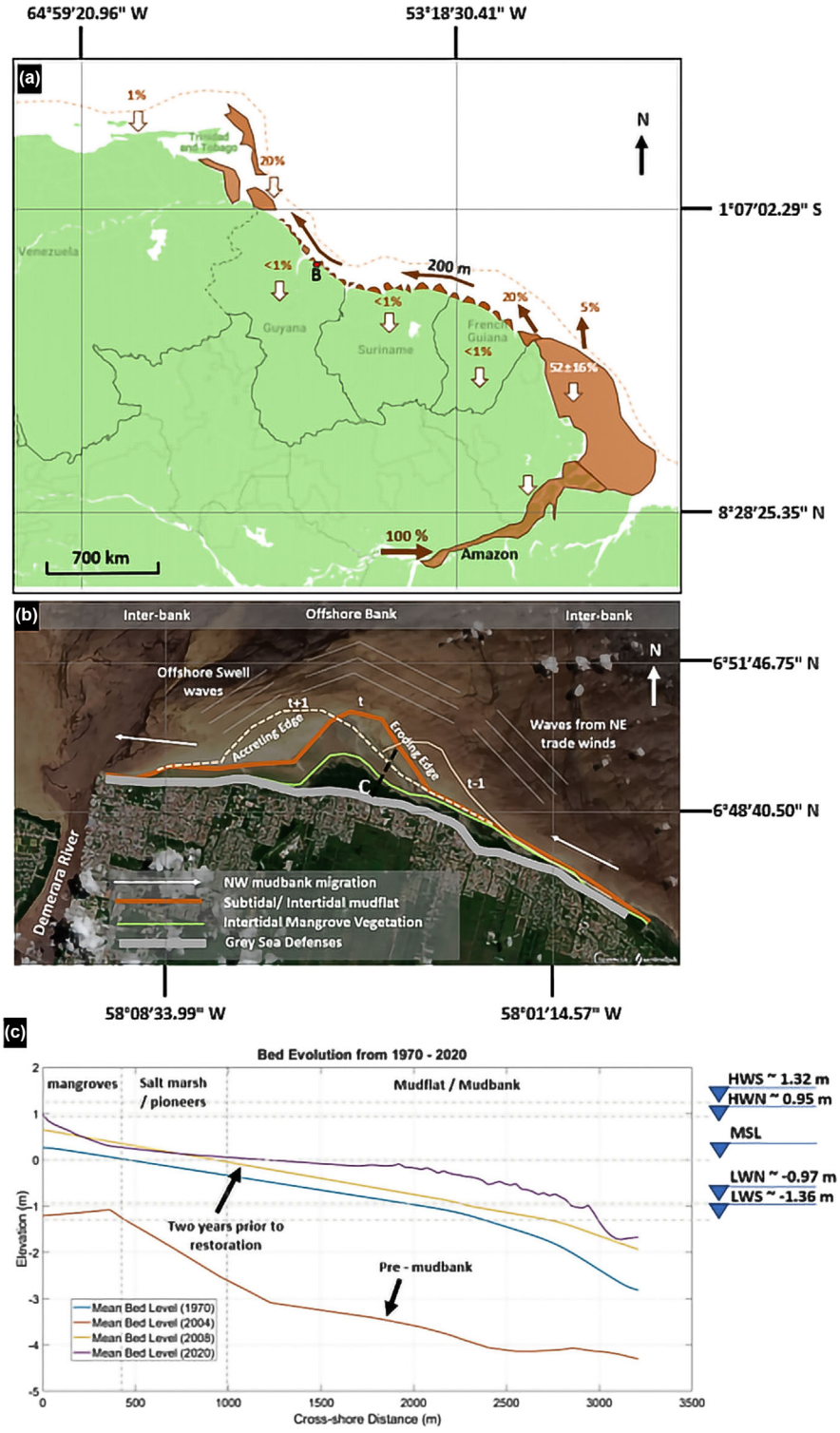

FIGURE 1 Morphodynamic development in the mudbank – mudflat – mangroves Guyana coastal system. (a) The larger system dynamics along the Amazon Delta, Guiana coast and the Orinoco Delta and the fate of the Amazon-driven suspended sediment (Allison et al., 2000; Allison & Lee, 2004; Meade et al., 1985; Milliman et al., 1982). (b) Factors governing the cyclic erosion and accretion patterns along the intertidal mudflat and mangrove fringe (NE = north east, NW = north west). (c) The evolution of the bed level spanning the mudbank cycle: pre-mudbank presence, with the mudbank, pre-restoration and almost 10 years post-restoration. Characteristic tidal water levels are indicated at the right axis (HWS = high water spring, HWN = high water neap; LWN = low water neap; LWS = low water spring) (Best et al., 2022b).

The analysis uses a MATLAB-based, numerical, 1D cross-shore profile model (Mflat: van der Wegen, Roelvink, & Jaffe, 2019) that includes high-resolution hydrodynamic and morphodynamic processes, extended with mangrove dynamics for the current study. Modelled conditions are validated against the data campaign carried out from 2019 to 2020 along the Guyana coast (Best et al., 2022b). The next sections describe the dynamics at the Guyana coast in more detail (setting, morphology and seasonal changes of the mudflat), the Mflat model setup, Mflat validation including an extensive sensitivity analysis of the model parameter space and the system's behaviour under constant forcing, cyclic boundary conditions and SLR.

2 | METHODOLOGY

2.1 | Study Site: System Dynamics & Field Measurements

The Guyana coast receives high sediment loads mainly from offshore mudbanks and, to a lesser extent, local river discharge, totalling 220–260 million tonnes annually. These sediments originate from the Amazon Basin and are transported along the northern coast of South America both as suspended loads and in migrating mudbanks (10–60 km long, 20–30 km wide, 5 m thick, migrate 1 to 1.2 km per year and spaced 25–50 km apart) in cycles of 20–40 years (Figure 1)

(Allison et al., 2000; Anthony, Gardel, & Gratiot, 2014; Eisma, Augustinus, & Alexander, 1991; Eisma & van der Marel, 1971; Gensac et al., 2015; Wells, Coleman, & Wiseman, 1978).

Bathymetry analysis of the Chateau Margot profiles (Figure 1c) revealed that during transitional periods (bank – interbank) volumetric differences in the mudflat per metre width can range from 9,000–12,000 m^3/m coastline in response to the presence or absence of the mudbank (Allison & Lee, 2004; Anthony et al., 2010; Anthony, Gardel, & Gratiot, 2014; Lefebvre, Dolique, & Gratiot, 2004). The transition between mudbank and interbank phases occurs over 5 to 15 years. Coastal retreat during interbank phases can reach 30–345 m per year (Augusseau et al., 2025; Augustinus, 2004).

Field data for model validation have been collected between November 2019 to January 2020 along the Chateau Margot coastline of Guyana, South America (Figure 1). The study site (6° 49′ 10.18" N, 58° 4′ 28.85" W) is located between two freshwater outfalls, approximately 9 km from the Demerara River and the capital city. The data presented in this paper are available open access via https://doi.org/10.4121/c.5715269 (Best et al., 2022a).

As described in Best et al. (2022b), this study site features a wave-dominated mangrove forest, exposed to both oceanic swells and semi-diurnal tides (1.17 m – 2.5 m). The Chateau Margot hinterland is approximately 1 m below mean sea level (MSL), and the several kilometres of mudflat extending offshore area are exposed during the low tide (Best et al., 2022b). The wave processes were extensively detailed along the transect, C shown in Figure 1 (Best et al., 2022b), where both swell (10–20 s) and infragravity (25–250 s) waves were observed, with wave heights varying between 20 and 80 cm and 5–10 cm, respectively. Mud damping and depth limitation contribute significantly to the wave attenuation by 85–90% over the mudflat from offshore to the mangrove-mudflat edge. Within the first one-third of the fringe width (120 m), the mangroves further reduce the wave height by 50% (Best et al., 2022b).

Incident waves typically originate from the northeast, with an average significant wave height of 1.25 m to 2.25 m and a historical maximum of 4 m. The peak wave period ranges from 6 to 10 s, averaging 7.5 s, but can increase to 16 s from September to April due to tropical storms, hurricanes and depressions in the Atlantic Ocean and Caribbean Sea.

Best et al. (2022b) mapped the intertidal topography (1,000 m × 3,500 m) of the study site using high-resolution precision instruments along 11 transects at 10 m intervals. The site features a mangrove platform, elevated 0.1–0.5 m above MSL, with a small fronting cliff separating the mangrove forest from the mudflat. Tidal creeks and the mangrove forest lie adjacent to a concrete seawall that protects 85% of the Guyana coast. The site has silty clay soil with sediment concentrations exceeding 5 g/l, varying between 40 g/l to 60 g/l along the mudflat.

The area (Figure 1b) was restored by the Guyana Mangrove Restoration Project with the planting of 13,000 seedlings in 2011. The *Avicennia germinans* has established itself as the dominant species with the secondary establishment of *Languncularia racemosa*, *Rhizophora mangle* and salt marshes. High-resolution vegetation data were transformed into vegetation cover maps (Best et al., 2022b). The maximum stem diameter and height for the *Avicennia* were 12 cm and 13 m, respectively, while the *Languncularia* had a maximum diameter of 7 cm and a height of 12 m.

2.2 | Model Description

Our modelling effort focuses on a description of the mudflat dynamics <=3.5 km from the coastline, while the mudbank dynamics impose the boundary conditions for our model. Mflat features both the cross-shore hydrodynamics as well as a stationary wave model on a high-resolution grid (dx = 10 m) and the time period (dt = 5 s). This is achieved through the simplified application of the shallow water equations with the added benefit of fast computation times (van der Wegen et al., 2017). The vegetation dynamics follow the windows of opportunity concept as outlined by Best (2017) and Legay (2020), and as detailed in the paragraphs below. The mass balance equation (van der Wegen et al., 2017; van der Wegen, Roelvink, & Jaffe, 2019) governs the determination of the cross-shore velocities since the assumed low velocities allow for the neglection of the inertia and friction terms in the momentum equation. Due to the relatively calm wave conditions, H_s = 0.1–0.5 m, associated with the presence of mudbanks along the Guyana coast (especially in the subtidal and intertidal zones), the wave-driven longshore flow and the impact of the waves on the longshore shear stress are neglected. We use shore normal wave conditions and assume that longshore components refract further offshore, allowing for the perpendicular incidence. An advection–diffusion equation solves cross-shore sediment transport while the bed level changes occur by the divergence of the sediment transport field. The wave energy profile over the mudflat is determined using the stationary wave energy balance, allowing for wind energy supply, wave breaking and dissipation by bed and vegetation friction (van der Wegen, Roelvink, & Jaffe, 2019). Since this region is governed by fine cohesive sediments, the Partheniades-Krone formulations are used to determine sediment erosion and deposition (van der Wegen, Roelvink, & Jaffe, 2019). The combined sediment transport gradients and the erosion and deposition terms, enhanced by the morphological factor (MF) determine the changes in the bed level.

The vegetation is imposed across the 1D grid domain, through the definition of three new variables (mangrove height, diameter, number of plants- See Figure 2). The optimal tree growth is described using a sigmoid function correlating the actual tree size (diameter and height) and the upper limit of the tree size (D_{max}, H_{max}). The depression of the tree growth rate under less than optimal conditions (e.g. strong competition of neighbouring trees and increased inundation duration) is considered through multipliers or limiters which act to correct the optimal function. This multiplier or limiter has a range between 0 (least favourable conditions) and 1 (optimal conditions). Following Berger & Hildenbrandt (2000), Shugart (1984) and Chen & Twilley (1998), the growth of the mangrove trees with the decay multipliers is described by:

$$\frac{dD}{dt} = G.D\,\frac{\left(\frac{1-D.H}{D_{max}.H_{max}}\right)}{274 + 3b_2.D - 4b_3.D^2}\,(IC) \tag{1}$$

$$H = 137 + b_2.D - b_3.D^2 \tag{2}$$

where D is the mangrove trunk diameter [cm]; b_2 and b_3 are species-specific growth constants in the height-to-dbh relationship; G is the species-specific growth parameter [cm/yr.]; D_{max} is the maximum

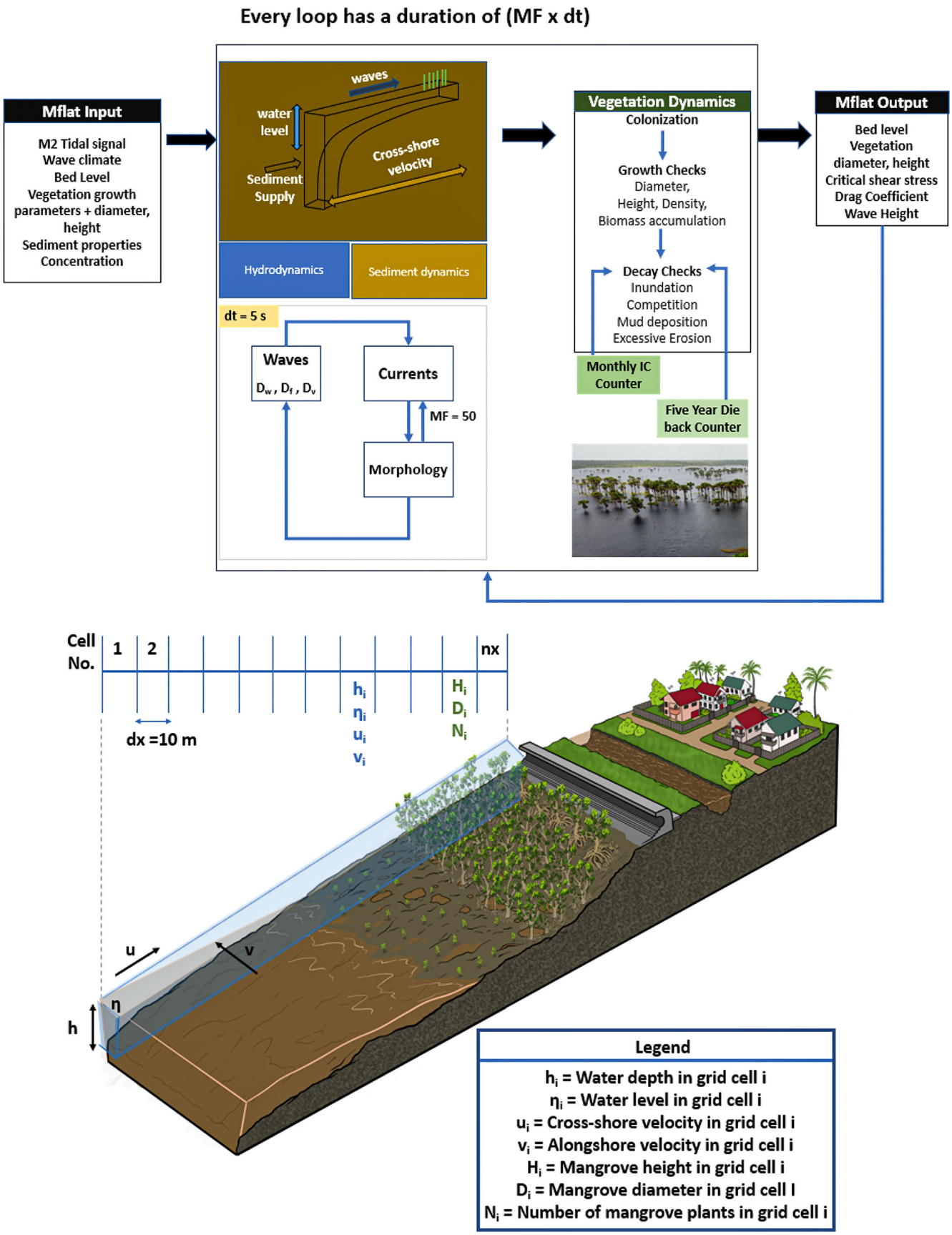

FIGURE 2 (a) Mflat – Mangrove coupling methodology for the long-term modelling of the interaction between the vegetation growth, tide, waves, sediment transport and biomass accumulation. (b) Conceptualization of the modelled vegetation and model variables along the Guyana coastline along the 1D grid.

TABLE 1 Comparison of available theoretical and measured property datasets post-restoration for the model set-up for *Avicennia germinans* mangrove-mudflat representation, where d.b.h is the diameter at breast height.

Parameters	Description	Theory 60–70 years	Sources for theoretical values	Measurements, 10 years post
N	Number of mature plants (100 m^2)	1	(Chen & Twilley, 1998, Fontalvo-Herazo et al., 2011, Piou et al., 2008)	70
G	Growth parameter (cm/year)	162	(van der Wegen et al., 2017, Shugart, 1984, Mendez & Losada, 2004, van Rooijen et al., 2016)	750
D_{max}	Maximum d.b.h (cm)	40–140	(Mendez & Losada, 2004, Shugart, 1984, van der Wegen et al., 2017)	20
H_{max}	Maximum height (cm)	1700–3,500	(Mendez & Losada, 2004, Shugart, 1984, van der Wegen et al., 2017)	1,400
b_2	Constant in height to d.b.h relationship $= 2(H_{max} - 137)/D_{max}$	48.04	(Mendez & Losada, 2004, Shugart, 1984, van der Wegen et al., 2017)	136
b_3	Constant in height to d.b.h relationship (cm^{-1}) $= (H_{max} - 137)/D^2_{max}$	0.172	(van der Wegen et al., 2017, Shugart, 1984, Mendez & Losada, 2004, van Rooijen et al., 2016)	3.5
H_{pneu}	Height of the pneumatophores (cm)	15	(Chen & Twilley, 1998)	10
D_{pneu}	Diameter of the pneumatophores (mm)	1.0	(Chen & Twilley, 1998)	2.6
f_{pneu}	Coefficient for the calculation of the number of pneumatophores (−)	0.300	(Chen & Twilley, 1998)	0.274
$D_{0.5}$	Stem diameter (cm)	20	(Chen & Twilley, 1998)	20
S	Maximum number of sapling recruits per plot per year	30	(Chen & Twilley, 1998, Fontalvo-Herazo et al., 2011, Shugart, 1984)	30

diameter in the growth process [cm]; H_{max} is the maximum height that can be achieved [cm]; H is the mangrove height [cm]; I is the inundation stress parameter [−]; C is the stress due to competition for resources [−]. The species-specific parameters G, D_{max}, H_{max}, b_2 and b_3 are provided for the *A. germinans* in Table 1. Table 1 compares the theoretical growth parameters for a mature *Avicennia* tree (40–50-year-old) to the growth parameters for 10-year-old *Avicennia* trees along a restored site in Guyana. The latter was used in validating the changes in the diameter, height and spacing of the trees in the model. Young saplings which establish in the model have a diameter of 1.37 cm and a height of 137 cm.

Mangrove growth is monitored both monthly and over a five-year span using an IC counter. Trees die when the IC value, a decay multiplier, drops below 50% of optimal conditions. The decline in mangrove density and biomass, as well as the effects of high inundation stress and reduced resources, are detailed in the supplemental materials, ultimately leading to one mature *A. germinans* mangrove per 100 m^2 (Berger & Hildenbrandt, 2000; van Maanen, Coco, & Bryan, 2015).

2.2.1 | Mangrove influence on the physical processes

The mangrove growth dynamics influence hydrodynamics and sediment dynamics in the following ways:

- Increase the critical erosion shear stress: It is considered that the critical erosion shear stress τ_{cr} linearly increases with the mangrove vegetation below-ground biomass (Mariotti & Fagherazzi, 2010).

$$\tau_{cr} = \tau_0 . \left(1 + K_{cr} . \frac{W_{bg}}{W_{bg.max}}\right) \quad (3)$$

where τ_0 is the critical shear stress without vegetation [N/m^2]; K_{cr} is a dimensionless coefficient = 0.1; W_{bg} is the below-ground biomass; $W_{bg.max}$ is the maximum below-ground biomass. Further details on the parameters can be found in the supplemental material.

- Increase the drag coefficient C_D. This effect is incorporated by defining C_D as a function of the projected area of mangrove vegetation and the volume of the vegetation (Mazda et al., 1997). As a result, mangroves influence tidal flow velocities and thus affect the magnitude of sediment transport (Nardin, Edmonds, & Fagherazzi, 2016).
- Increase the bed level by organic matter accumulation: The decomposition of the refractory component of the organic matter is very slow, allowing for the build-up of the soil elevation by 1 mm/yr. (Morris & Sundberg, 2024; Swales et al., 2015; van Maanen, Coco, & Bryan, 2015). This is a conservative estimate based on field measurements of other species (Chapman & Ronaldson, 1958; Mckee, 2011; Saad et al., 1999; Spenceley, 1977; Swales & Lovelock, 2020; Xie et al., 2023).
- Decrease in the wave impact: The vegetation influence on the waves is added by considering an additional dissipation term D_v in the Mflat stationary wave energy balance (Mendez & Losada, 2004). The equation below accounts for the impact on both the mangrove trunk and pneumatophores and not the canopy since water depths do not reach such levels.

$$D_v = \frac{1}{2\sqrt{\pi}} . \rho . \widehat{C}_D . D . \frac{N}{dx^2} . \left(\frac{k.g}{2.\ \omega}\right)^3 . \frac{sinh^3(k.\ H_{uw}) + 3\sinh(k.\ H_{uw})}{3.\ k.\ cosh^3\ (k.h)} . H^3_{rms} \quad (4)$$

where k is the wave number [rad/m]; g the gravitational acceleration [m/s^2]; ω the wave frequency [rad/s]; h the water depth [m]; H_{uw} the

submerged mangrove height [m]; $\hat{C}_D$ the bulk drag coefficient = 0.4 [−] (van Rooijen et al., 2016; Mendez & Losada, 2004). This bulk drag coefficient is subject to calibration dependent on the mangrove species.

Further details regarding the equations and implementation of these effects can be found in the Supporting Information.

2.3 | Model Setup and calibration

2.3.1 | Domain and Topography

The overall model setup describes a 1D section of a mangrove-mudflat system, 3,500 m cross-shore with 10 m grid cells. The typical initial profile was derived from the data set presented in Best et al. (2022b) and is patterned after the 1970 bathymetry of the Chateau Margot field site (Figure 1c). The direction of the profile was approximately aligned to the wind and wave direction during extreme wave heights to compare the simulated dynamics of the mangrove edge with field observations and discuss the effectiveness of the green-grey infrastructure in damping the wave energy. The bed increases from −3.5 m at the seaward boundary (only open boundary) to 0.3 m at the landward edge of the mangrove fringe over a cross-shore distance of 3,500 m.

2.3.2 | Boundary Conditions and other Model Parameters

With the aim of testing the numerical stability of the model and exploring the existence and conditions of equilibrium of the mudflat-mangrove system, the model was forced only with an M2 water level boundary at the seaward edge with an amplitude of 1 m.

Secondly, schematizing migrating mudbanks in the definition of the boundary conditions was more of a challenge. Ideally, the model domain would cover the mudbanks and extend 20–30 km, but this led to excessive computational efforts. Therefore, we consider the relative changes that are observed at a 3.5 km distance offshore. These conditions are then indirectly determined by the larger migration process.

Our 3.5 km long model is much shorter but, as a consequence, needed boundary conditions reflecting the dynamics at the mudflat that were, a priori, not known. We assumed that the impact of migrating mudbanks could be described by cyclically (sinusoidally) varying wave heights, wave periods and suspended sediment concentrations at the boundary (Allison & Lee, 2004; Anthony et al., 2010; Winterwerp, Borst, & de Vries, 2005). These then represent the gradual dynamics from mudbank phases (a smaller wave height/period and higher sediment concentration) to interbank phases (a larger wave height/period and lower sediment concentration). Preliminary modelling suggested that the observed mangrove belt extent and cyclicity could be represented by the cyclic boundary conditions with significant wave heights (H_s sinusoidally varying between 0.1 and 0.5 m), wave periods (T_p sinusoidally varying between 4.4 and 5 s) and suspended sediment concentration (SSC sinusoidally varying between 0.35 and 0.45 kg/m^3). These value ranges were roughly in line with scarce observations (Augustinus, 1987; Best et al., 2022b; ICBA, 2006; van Ledden et al., 2009; Welage, 2005). The base model does not include longshore flow. Erosion occurs at a rate of 8×10^{-5} kg/m^2/s in cells with shear stresses exceeding a critical shear stress of 0.18 N/m^2. Deposition occurs at a rate of the product of the settling velocity (w = 1.2 mm/s) and the local SSC.

Within the context of this research, equilibrium will depend on both the vegetation dynamics and the geomorphological developments. For the geomorphological development aspect, equilibrium refers to a profile which has a dynamic nature, including suspension and transport of sediments during a tidal timescale, albeit with no tide residual development, so that the profile remains morphologically stable after a tide. Depending on the initial bathymetry and forcing, this equilibrium can be reached within decades (van der Wegen, Roelvink, & Jaffe, 2019). Typically, mangroves attain a dynamic equilibrium density after 50–70 years (Fromard et al., 1998). To capture and explore equilibrium conditions, the model run duration therefore extends to at least 100 years (see Table 2 for parameters).

3 | MODEL RESULTS

First, we explore the conditions of equilibrium using a simplified M2 tidal forcing only to bridge the connection with existing literature on

TABLE 2 Calibration parameters for the base model simulating the mangrove growth and migrating mudbanks along the Guyana coastline.

Parameter	Description	Value	Units
MF	Morphological factor	50	-
H_{rms}	Root mean square wave height	0.1–0.5	m
T_p	Peak wave period	4.4–5	sec
bcs	Sediment concentration at the sea boundary	0.35–0.45	kg/m^3
ww	Settling velocity of the sediment	0.0003	m/s
τ_{cr}	Critical shear stress for erosion	0.17–0.3	N/m^2
Ch	Chézy friction factor	60	m$^{1/2}$/s
gamma	Breaking index	0.60	-
fmd	Percentage dissipation of energy due to fluid mud	0.000	-
kb	Wave friction-related parameter	0.004	-
wdf	Wave dissipation reduction factor, e.g., by fluid mud	1	-
MM	Erosion factor	0.00008	kg/m^2/s

equilibrium conditions. We then add complexity by cyclic forcing conditions representing the observed nearshore conditions of the mudbank migration. This consists of the first step in studying the consequences of mudbank migration on nearshore mudflat profiles. We analyse in detail the intertidal flow, sediment, wave and mangrove dynamics on the mudbank and interbank profiles and discuss the morphodynamic inertia under cyclic conditions. This is followed by an extensive sensitivity analysis of applied bio-geomorphological model parameters, including sediment properties, vegetation presence and full harmonic components. Finally, SLR scenarios are discussed.

3.1 | Equilibrium development of the M2-dominated mangrove-mudflat system

Figure 3 depicts the bio-geomorphological development of an M2 tidal-driven mangrove-mudflat system (along a 3,500 m profile) over 170 years with either cyclic boundary conditions (H_s, T_p, bcs- lower panels) or constant boundary conditions (upper panels). In both cases, the temporal and spatial variations of the mangrove diameter, height, number of plants, inundation, competition and overall growth limiters, along with the bed level and wave height are presented for both non-cyclic and cyclic systems.

Mflat is able to generate equilibrium profiles and vegetation distributions for both constant and cyclic boundary conditions. For the constant boundary conditions, Figure 3 shows that the M2 tidally driven non-cyclic system develops to a point of equilibrium within 60 years. During the initial phase of the mudflat build-up, the geomorphological development leads to mangrove colonization and growth, as shown by the developments in the height, diameter and density of mangroves. Note that mangroves will not establish on a bed level below the mean water level since the growth limiter is below 0.5 in this zone. The equilibrium profile develops between the seaward and landward edges. Starting from an initially deep mudflat bed level, mud deposits near the seaward boundary during flooding of the profile. The mudflat profile continues to accrete until the time when erosion by wave action at low water balances with bed accretion during flood. At these equilibrium conditions, tide-varying SSC levels and bed level changes still occur, albeit that there is no tide-residual morphodynamic effect (van der Wegen et al., 2017). Comparison of the constant and cyclic forcing conditions (Figure 3) shows that equilibrium conditions under M2-only tidal forcing (Figure 3a–h) also develop for a mudflat/mangrove system. Systems with cyclic forcing (Figure 3i–p) initiate a dynamic equilibrium with a period in the order of decades.

The cyclic system displays regular growth and decay patterns of bathymetry and mangrove belts. Figure 4 compares the geomorphological developments of the models with constant (a, d) and cyclic M2 tide-driven forcing (b, e), and cyclic tidal-driven forcing with full harmonics (c, f) along cross sections at specific points. The profile shape for the cyclic tidally driven system with full harmonics undulates between concave and convex profiles. The concave forming forcing (eroding) peak after 10 years of mangrove presence, while the convex forming conditions begin shaping the profile 5–6 years after the mangroves have disappeared. After 90 years, constant interbank and bank profiles have formed with maximum intertidal elevations of −1.5 m and 1 m, respectively.

Within constant tidally driven M2 forcing, there is a temporal disparity along the profile where the upper intertidal area attains morphodynamic equilibrium first, while the lower sections attain the same after 80 to 100 years (Figure 4a,d). Additionally, there is a delay between the morphological equilibrium and the vegetation growth platform where the seaward portions of the fringe are still maturing and do not attain the maximum growth range until 100 years. The landward sections, however, quickly mature due to the higher bed elevation. In the case of the full harmonics, the deposition of sediment occurs first along the seaward extents of the transect (Figure 4c,f), and then the depositional wave migrates cross-shore to the vegetated sections. The build-up of the mangrove areas is noticeable from the third mudbank cycle, after which the profile continues to evolve.

The cyclic system shows morphodynamic inertia where sections closer to the seaward boundary respond to changes sooner than more landward located sections. Maximum bed level at the landward end is reached about 10 years after the maximum bed level near the seaward boundary occurs. It is important to note that the cyclic forcing does not reach equilibrium profiles belonging to the equivalent maximum and minimum constant forcing conditions. In other words, the cyclicity is of a shorter duration than the morphodynamic adaptation timescales required to reach the equilibrium state of the boundary forcing conditions end members.

3.2 | Mangrove dynamics

In Mflat, the growth is initiated with sparsely, randomly placed young seedlings, which then increase in diameter and height until a dense forest of very mature trees forms after 100 years. The *Avicennia* mangroves naturally prograde to newly elevated intertidal areas, while the landward sections become sparsely populated as the upper limit of the allowed hydroperiod is reached (see Figure 3 for the IC values). Along similar sections of coastal mangroves in Guyana, they are outcompeted by the *Languncularia racemosa* (Best et al., 2022b). Contrastingly, mangroves along cyclic systems rarely reach their full maturity in Mflat. In the non-cyclic M2 case, the removal of the tree, without the representation of terrestrial species, may result in an underestimation of the wave attenuation along the most landward extent of the intertidal area. Trees colonize the upper mudflat and grow in a similar fashion as under the non-cyclic forcing. After two-thirds of the mudbank cycle, the mangrove diameter and height begin to exceed 60 cm and 7 m, respectively. During the transition to the interbank phase, the vertical and horizontal extent of the developing platform limits the inundation stresses. During the interbank phase, the conditions do not allow for the survival of the vegetation. The timescale for the maturity of the mangroves is, however, longer than the mudbank cycle, and plants do not attain full maturity before the environmental conditions are no longer sustainable for growth. Therefore, the conditions for the optimal stabilization and biomass accumulation of the mudflat profile are never realized in the modelled cyclic systems.

With mangrove vegetation, the interface between the bare mudflat and the mangrove fringe, along with the seaward half of the fringe, is heightened from 0.1 m to 0.3 m compared to the run excluding vegetation dynamics. The elevation within the landward half of

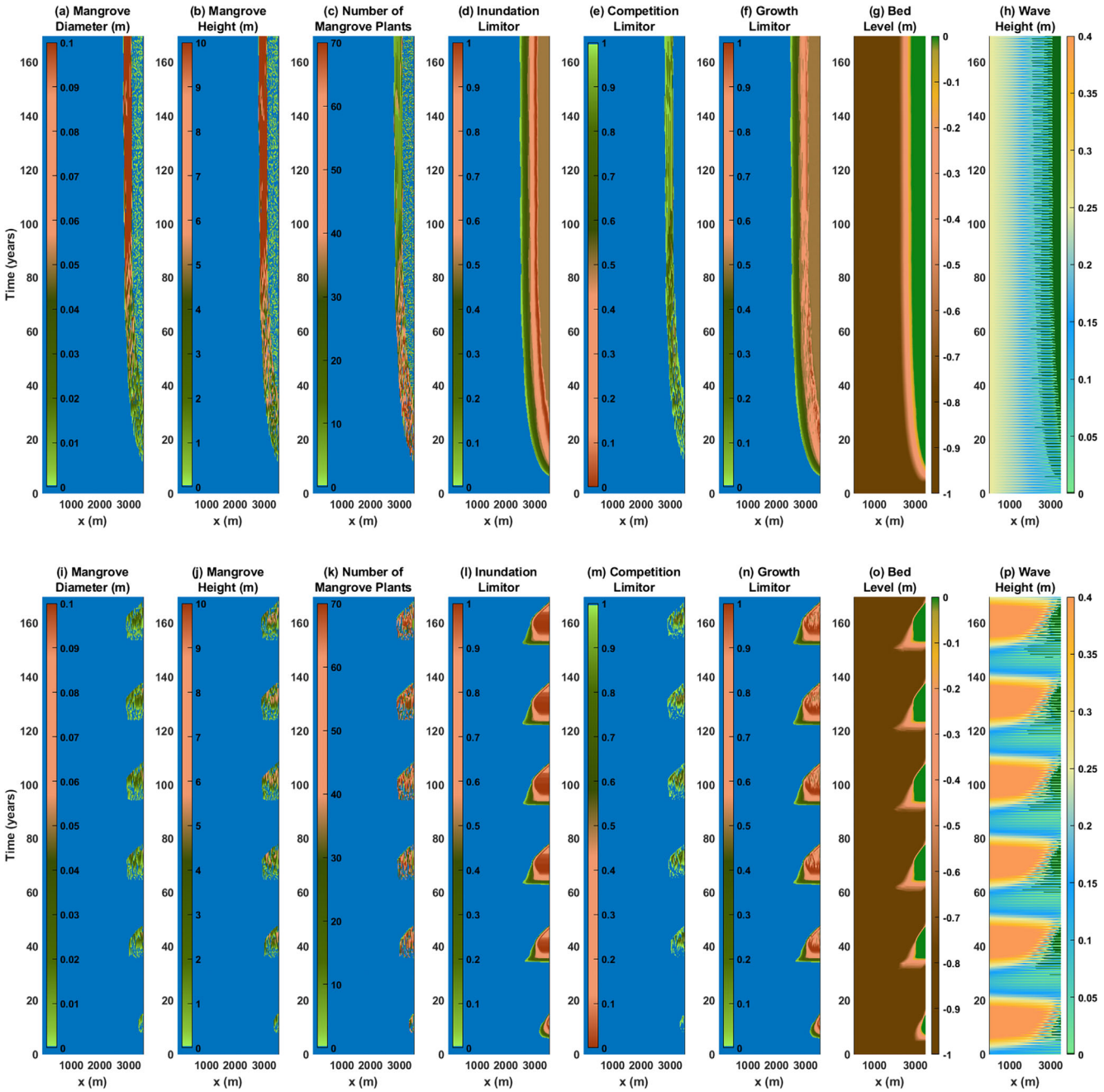

FIGURE 3 Model Performance for the (upper panel) non-cyclic M2 tidally driven system and a cyclic M2 tidally driven system (lower panel), where the morphological and vegetation dynamics are analysed along with cross-shore wave height variation for a period of 170 years.

the fringe has minimal variation. This suggests that the impact of vegetation remains quite limited compared to the morphodynamic behaviour of the system under cyclic forcing. For non-cyclic forcing, the height between the vegetated and unvegetated profiles differs by 0.1 m, but the width of the platform is three times longer with vegetation.

3.3 | Intertidal dynamics

Figure 5 shows the intertidal dynamics on the 'mudbank' and 'interbank' profiles at 2-hr intervals during a complete tide. At these intervals, the processes analysed include the cross-shore velocity, wave height, flow-induced shear stress, wave-induced shear stress, total shear stress, concentration and bed level change (Figure 5a,b). Compared to the observed bed level differences seen in profiles from 1970 to 2004 gathered during the data campaign (Figure 1c), there are similarities with the modelled vertical bed level range resulting from the mudbank cycle. In Figure 5a, the interbank forming processes, e.g. increasing wave heights and shear stresses initiated by the longshore mud transport, begin to erode the vegetated mudflat.

Figure 5b shows the profile which results from these eroding processes, and at this point, the processes that once resulted in the erosion of the profiles have now reduced (decreasing wave heights and shear stress), instigating the formation of a new mudbank profile. Further analysis of the profile changes, as the dominating processes fluctuate in the mudbank cycle, reveals that the interpretation of the

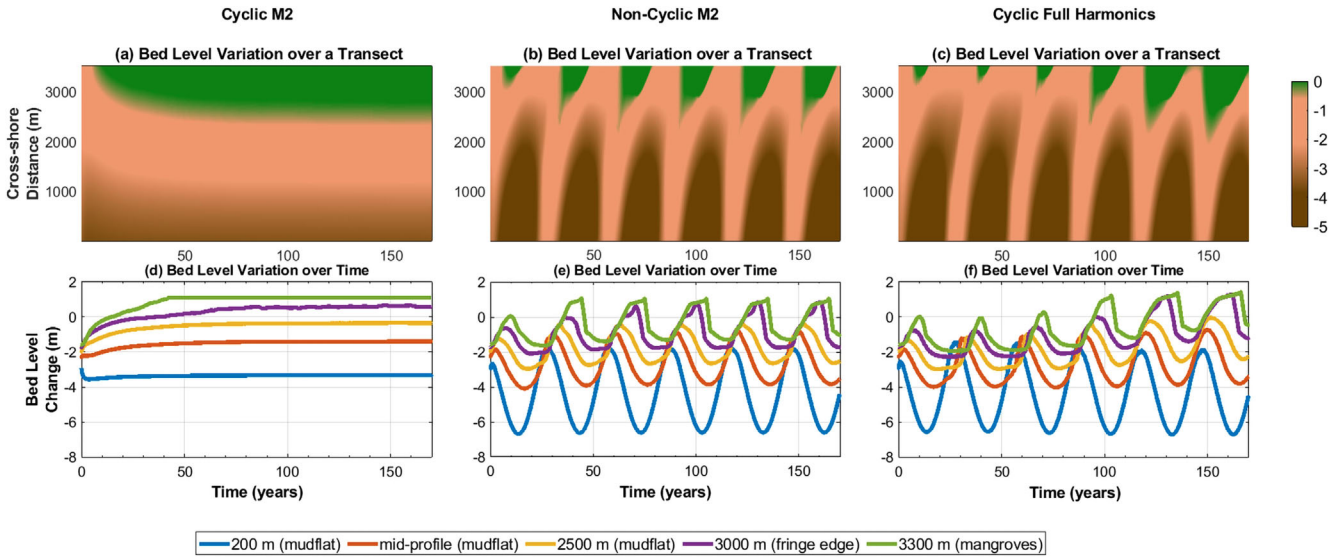

FIGURE 4 The spatial and temporal development of the bed level profile over 170 years, showing conditions under (left) Non-Cyclic M2, (middle) Cyclic M2 and (right) Cyclic Full Harmonics. The mid-profile location is taken at 1750 m.

profile shape is linked to its position within the mudbank cycle. For example, the concave profile observed in Figure 5a, though once accreting, is now dominated by eroding forcing.

During the mudbank phase, model results show a platform at the landward end that is mangrove-covered. This platform also emerges without vegetation dynamics and is the result of mudflat morphodynamics. Waves primarily erode the bed profile in Figure 5a, resulting in the entrainment of sediments during falling tide, as indicated by the erosion of the intertidal area in excess of 1 m. The modelled wave heights and flow velocities aligned well with field observations reported at stations along the transect (Figure 5a). Wave heights ranging from 0.4 to 0.5 m were observed in the field at depths of −2 m while flow velocities over the nearshore mudflat averaged 0.2 m/s. In Figure 5a, waves heights of 0.4 m are observed slowly eroding the platform with wave-induced shear stresses exceeding 2 N/m^2 during high water.

Within the interbank phase, neither intertidal area nor mangroves are present due to the reduced bed elevations. Along this profile, the cross-shore velocity modelled ranged between ±1.2 m/s, which corresponds well to studies along the coast of Guyana and French Guiana at depths exceeding −6 m. However, as the wave heights reduce due to increasing sediment volumes, the profile naturally accretes. As the mudflat continues to accrete waves dissipate most of their energy offshore and increase the suspended sediment volume.

In this case, higher concentrations are transported to the intertidal area during the rising tide and settle during calm conditions. The flow-induced shear stresses provide a higher contribution (> 2N/m^2) to the overall bed shear stress, and this is accompanied by positive bed level changes up to 1 m.

Vegetation dynamics from field observations (changes the diameter, height and density) during the average 20–30 yr. cycle show that the *Avicennia* has a maximum diameter and height of 0.12 m and 13 m, respectively (Figure 3). These extremes are visible in the system with constant forcing as the vegetation is allowed to mature. Within the cyclic system, the diameter corresponds well, but the mangrove heights are lower, with a maximum of 8–9 m. The vegetation presence along the heightened landward edge of the mudflat reduces the velocities and the wave heights by more than 90% within the first half of the fringe width (200–250 m). Observed patterns revealed that a belt width of 120 m already reduces the wave heights by 50%; therefore, the modelled results are within range. Within the fringe, the modelled velocity values ranged from 0.01 to 0.05 m/s, while on the mudflat, they were between 0.1 and 0.2 m/s, both of which correlated well with the results of Furukawa, Wolanski, & Mueller (1997) and van Maanen, Coco, & Bryan (2015).

Observed suspended sediment concentrations typically exceeded 1 g/l with a maximum of 60 g/l. However, these values were not reached within the model computations. Within the model, concentrations were up to 4 g/l along the upper intertidal area. The high concentrations may eventually lead to fluid mud that has a great potential of dissipating wave energy. Occurrence of fluid mud has indeed been observed along stretches of coast but this process was not included in the model.

3.4 | Model parameter sensitivity analysis

Figure 6 presents the key model parameters which influence the geomorphological developments of the mangrove–mudflat profile: wave height and period, critical shear stress, wave dissipation, concentration, tidal range, settling velocity, vegetation seeding frequency, age of the trees and vegetation-induced drag. Here we observe that a deeper profile with a narrower mangrove fringe is reached when applying a larger wave period, a lower critical shear stress and a lower settling velocity. This corresponds to conditions where sediment is easily suspended. A lower SSC boundary condition value also leads to a deeper profile because less sediment is supplied to the domain each flood. A high wave dissipation factor (wdf) attenuates waves faster, thereby creating wider platforms for mangrove colonization. In the absence of a fluid mud layer, high wdf factors increase the bed shear

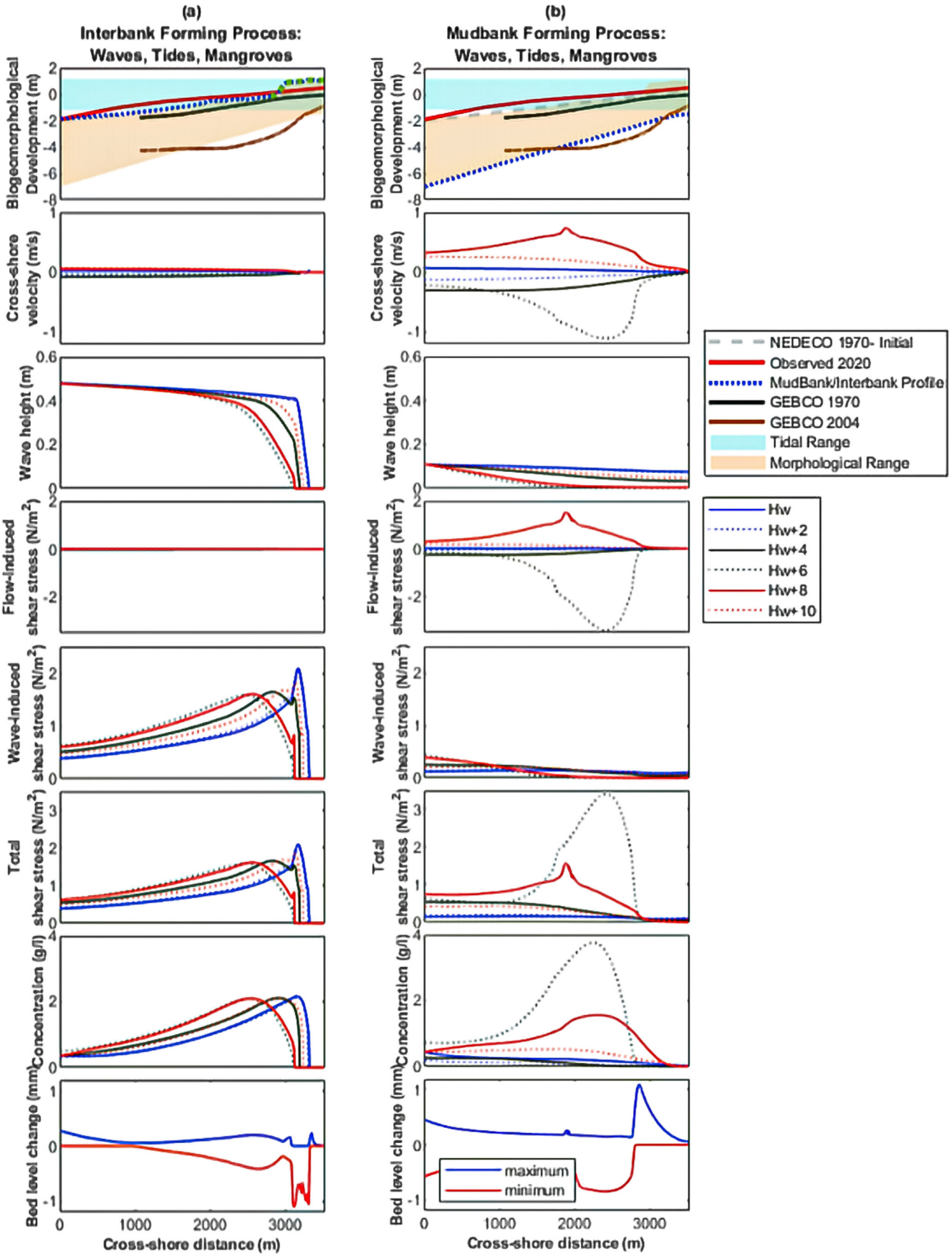

FIGURE 5 Intertidal dynamics on the 'mudbank' and 'interbank' profiles at 2-hr intervals during a complete tide in terms of cross-shore velocity, wave height, flow- and wave-induced shear stress and total shear stress, concentration and bed level change across the 3,500 m profile. Here, the analysis focuses on the cyclic tidally driven M2 system, where (a) shows the conditions under which an interbank profile forms and (b) shows the same for a mudbank profile. A morphological factor of 1 was applied for the bed level changes to reflect the changes during a tide.

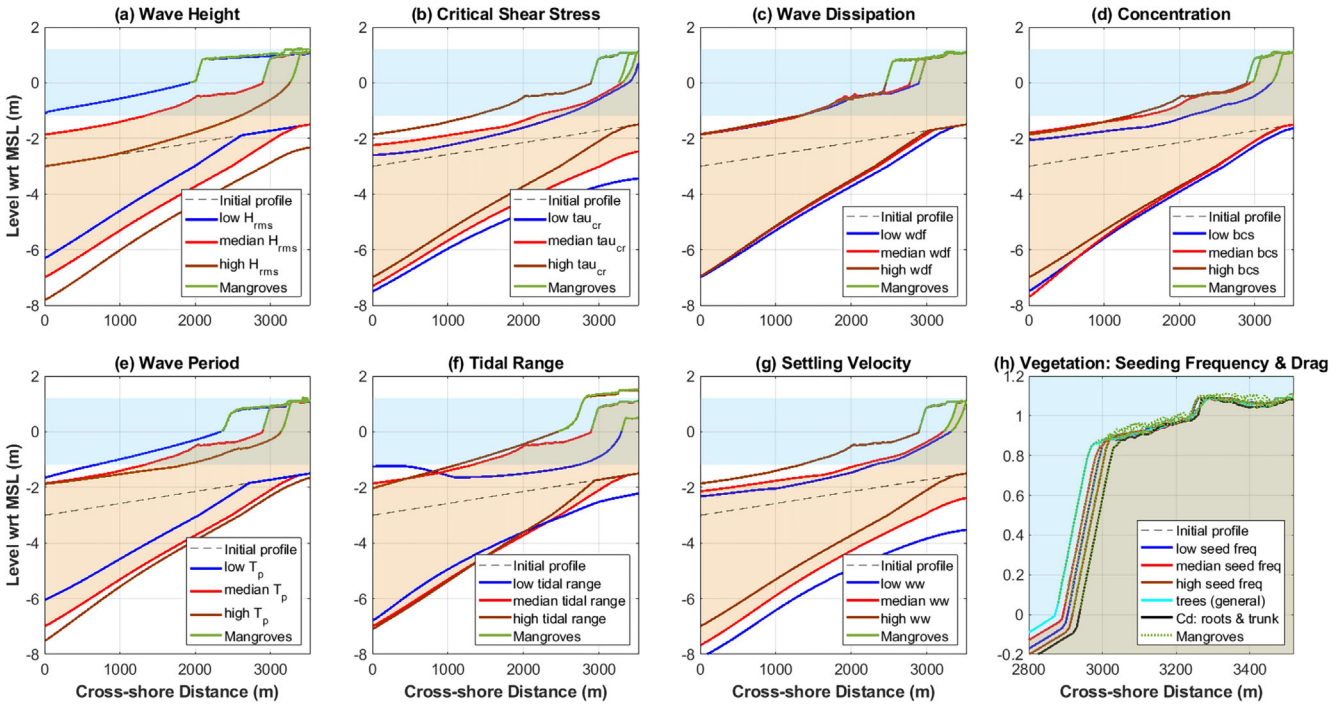

FIGURE 6 Sensitivity results panel summarizing the effect of variations in the key model parameters on the geomorphological development. Wave heights range from 0.02 m – 0.55 m, critical shear stress ranges from 0.09 N/m^2–0.17 N/m^2, wave dissipation ranges from 1 to 1.2, sediment concentration ranges from 0.2 kg/m^3–0.5 kg/m^3, wave period ranges from 3.4 s – 6 s, tidal range varied from 0.5 m – 1.5 m and the settling velocity varied from 0.15 mm/s – 0.3 mm/s. The vegetation sensitivity covers variations in mangrove seeding frequency (0.05–0.3), vegetation-induced drag ($D_{pneu} = 0.01$ m, $H_{pneu} = 0.15$ m, $e_{veg} = 10$) and the growth formula (general parameters for the *Avicennia germinans*). The two lines included for each variation in parameters indicate the highest mudbank and lowest interbank profiles, capturing the bed level change envelope.

stress for a given wave, and this leads to more erosion and a deeper profile in the morphodynamic feedback loop of the model. But along the Guyana coast, the extensive fluid mud layer (> 1 m) provides significant wave damping (Anthony, Gardel, & Gratiot, 2014).

The impact of the tidal range is less straightforward to interpret. A lower tidal range leads to a deeper profile at the landward region. This is obviously related to the maximum water level that can be reached during the tide at the landward end. However, the profile shows a contrasting behaviour at the seaward end, where a lower tidal range leads to a higher profile than a higher tidal range. This is because the accretion level at the seaward end is governed by wave action at low water, which is obviously lower for a larger tidal range. Sensitivity to vegetation parameter settings shows a very limited impact on the mudflat profile, with most impact along the seaward edge of the fringe. This suggests that mangroves, in this M2 model setup, act as opportunists following bed level development rather than as colonizers creating their own optimal environment. The findings provide realistic adaptation opportunities for restoration and protection works.

3.5 | Impact of vegetation, cyclic sediment supply & tidal components on morphology

Figure 7 highlights the influence of the mangrove presence and the tide on the geomorphological developments. This is shown first with the comparison of the cyclic M2 tidally driven system to the cyclic system driven by a tide with full harmonics. Both cases were analysed with and without vegetation. Figure 7a shows that a higher profile with a wider mangrove width is reached within the system forced by the tide with full harmonics. The mangrove presence widens the platform formed, and the platform extends further seaward with the full harmonics. With the full harmonics, the tidal non-linearity gives way to the increased landward transport. For non-cyclic systems, the vegetation presence heightens the platform for both M2 and full harmonics (Figure 7b,c). M2 cyclic systems, in this setting, show limited variation in the profile height and width with vegetation (Figure 7b). Under full harmonics, the cyclic vegetated systems produce wider platforms (Figure 7c).

Without mangrove vegetation, the edge of the platform is prone to higher levels of erosion. This is more pronounced along the seaward edge of the fringe, where the profile takes a concave shape with steeper transitions to the exposed and unvegetated sections. The mangrove presence has the greatest influence along the platform edge. In the cyclic case, the bed elevations along the upper intertidal area are quite similar for the vegetated and unvegetated cases. Less sediment is transported to this area when compared with the non-cyclic M2 and cyclic full harmonics scenarios, and the mangrove trees occupying this space remain there for less than 25 years. The latter results in a limited impact on the sediment transport and the bed level within vegetated areas. From the geomorphological perspective, mangroves occupy only a part of the tidal frame and are not a critical component. The observed differences in the width of the platform for the cyclic vegetated and non-vegetated scenarios are driven primarily by the geomorphological developments.

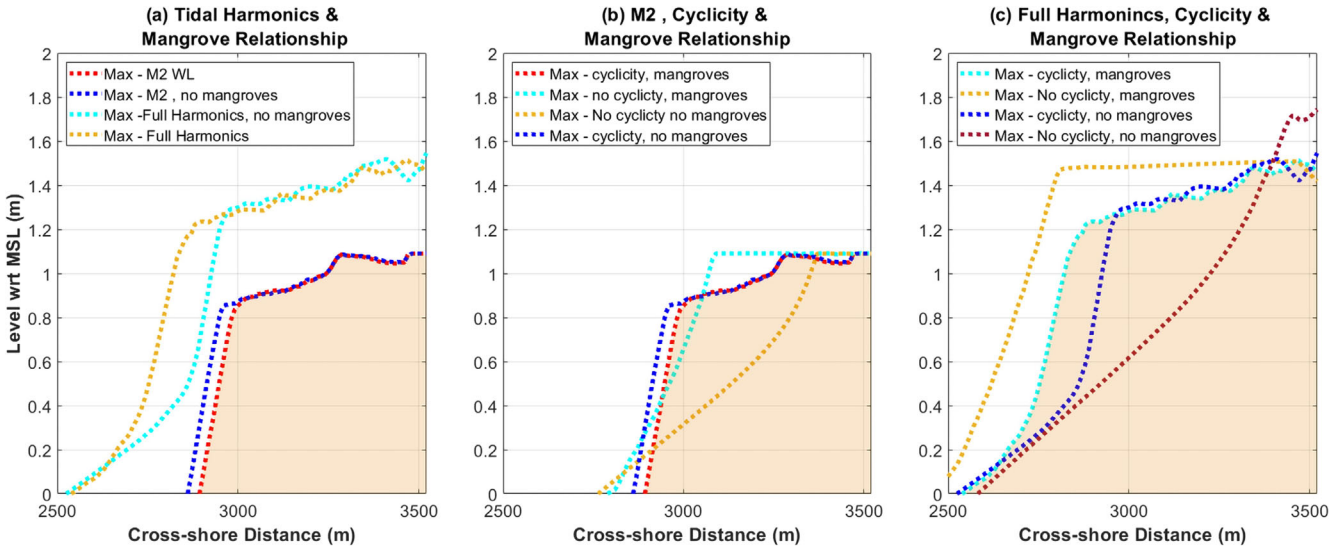

FIGURE 7 Evolution of the intertidal area of cyclic and non-cyclic tidally driven systems. We compare the bed levels to determine key trends in the geomorphological development under (a) varying tidal constituents, (b) both constant and cyclic M2 tidal conditions, with and without mangroves and (c) both constant and cyclic full harmonics tidal conditions, with and without mangroves. The patch in red represents the morphological range of the base run; however, we capture the bed levels only along the upper intertidal zone.

3.6 | The balance between migrating mangrove-mudflat and SLR

In this section, we analyse the resilience of systems with cyclic, non-cyclic and astronomic forcing under increases in the mean sea level ranging from 0.2 to 2 m. SLR is imposed via the boundary conditions after a 60-year spin-up period for a 100-year period. Figure 8 shows morphological development of the intertidal area and the wider mudflat at specific points under various rates of SLR. Figure 9 quantifies the loss of the intertidal area (viable areas for growth) for the cyclic M2 tidally driven system under 0.5, 1.0 and 2 m of SLR over the 100 years.

Under all four SLR scenarios, there is an increase in the loss of intertidal area (Figures 8 and 9), where despite bed increases that adapt to SLR, the width of the platform reduces. The remaining platform width in order of decreasing magnitudes includes systems with astronomic forcing, cyclic and then non-cyclic. In Figure 8a–d, steep transitions at the mangrove edge are visible along all profiles, but the platform disappears completely under 2 m SLR. This results in a landward shift of the mangroves to higher elevations to survive, where space is available. The larger tidal prism increases the flow velocities, thereby enhancing seaward erosion and landward deposition. Sediment is being transported from the mudflat onto the platform, which heightens but eventually drowns due to insufficient volumes. Cross-sections of the temporal evolution of the bed level reinforced that intertidal flat development is determined by the boundary conditions (Figure 8e–l). In all mangrove SLR scenarios, there was a level of inertia (lag effect in the time-varying bed level along the mudflat) in the system, which delayed the imposition of the boundary conditions on the upper profile.

After 100 years with 1 m SLR, only 50% of the intertidal area remains, while less than 30% remains for 2 m SLR. Initially, there is a high potential for adaptation over the first 40–80 years in all scenarios, but this soon fades. Moreover, under low rates of SLR, the positive bed level changes are confined to the platform, but this extends visibly to the mudflat for SLR increases in excess of 0.5 m. With increasing flooding depths, mangrove productivity and biomass accumulation potential increase (Cahoon, McKee, & Morris, 2021; Hogarth, 2015). Therefore, under SLR, for systems with higher organic accumulation rates (higher than 3 mm/yr.), there is a reduction in the loss of intertidal area and drowning rate (Figure 9). Overall the organic matter acted as a secondary contributor to the bed level with values ranging from 1×10^{-6} mm to 3×10^{-6} mm during the 30-year cycle. However, non-cyclic systems, where the trees are allowed to reach maturity, have a higher biomass productivity with values ranging from 10^{-1} to 10^{-2} mm for decadal simulations.

In simulations where the SSC is lower with higher wave heights, the rate of drowning and subsequent loss of intertidal area may reach 100% when SLR exceeds 1 m (Figure 10). However, here we assume that the wave conditions and the sediment concentrations remain the same, but SLR can also influence the magnitude of the waves and SSC, as well as the periodicity of the forcing. Therefore, we recommend that this provides an opportunity for additional optimization in future research.

Resilience in this context describes the drowning extent of the mangrove fringe and the rate of positive increases in the bed level elevation. With complex forcing such as the full harmonics, the rate of drowning is significantly reduced with higher and slightly steeper transitions from the platform (Figure 8d and Figure 10h). The final bed levels of the interbank profile are as expected, with higher bed elevations for increasing SLR rates (Figure 10d).

4 | DISCUSSION

In a 1D cross-shore manner, Mflat is adequately able to reproduce the cyclicity of mudflats and mangrove belts observed along the Guyana coast by varying SSC and wave height and period at the seaward

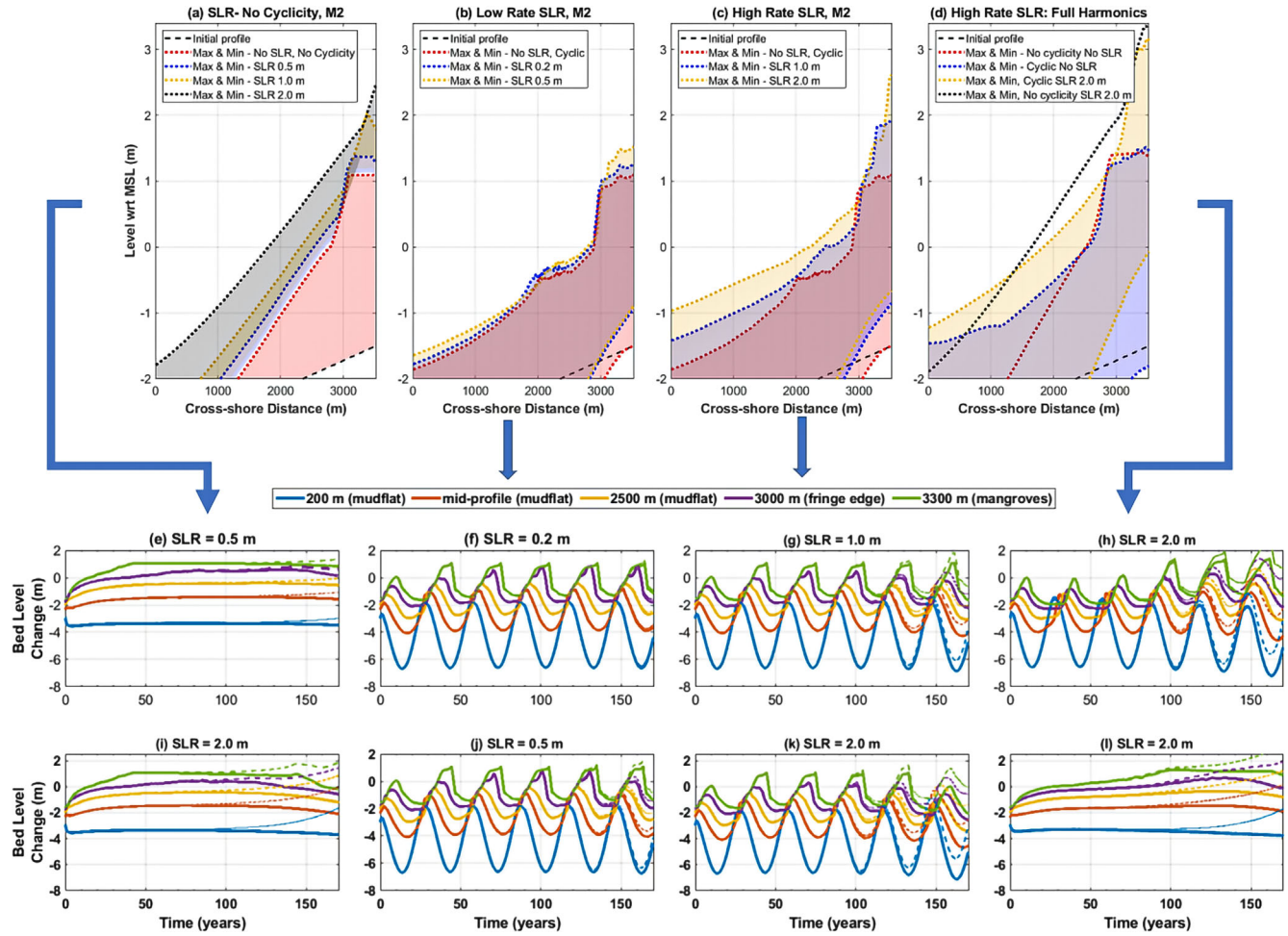

FIGURE 8 Evolution of the bed profiles across the intertidal area and over 100 years of sea level rise for both constant and cyclic tidally varying M2 and full harmonics systems. Panels a to d capture the spatial developments for (a) non-cyclic M2, (b) and (c) cyclic M2 and (d) cyclic and non-cyclic with full harmonics systems. Panels e to l capture the temporal developments for (e, i) non-cyclic M2, (f,g,j,k) cyclic M2 and (h,l) cyclic and non-cyclic with full harmonics systems. A datum correction by mean SLR has been applied to the solid lines in the lower panels, whereas the dotted lines do not include the datum correction.

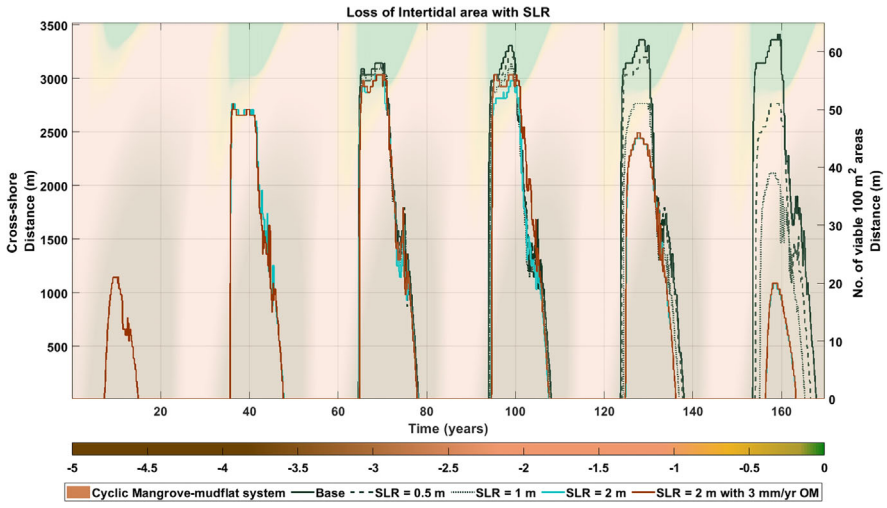

FIGURE 9 The comparison of the remaining intertidal areas under varying magnitudes of SLR (0.5 m, 1.0 m, 2.0 m). The intertidal area is defined as the number of viable growth areas (100 m^2) across the entire model domain each timestep for 170 years, wherein SLR is imposed from 100 years. The line displayed in brown shows the result of more productive mangroves, where OM refers to the organic matter. The background of this figure is a replica of Figure 4b bed level change (m) and provides the context for the expected changes with SLR.

boundary, mimicking the impact of the migration of the mudbanks on the mudflat. This was achieved through the interaction between the integrated bio-geomorphological approach that couples waves, tides, sediment transport and morphodynamics, with the growth, decay and organic matter accumulation of the *Avicennia germinans* mangrove species. The modelling approach was then utilized in the examination

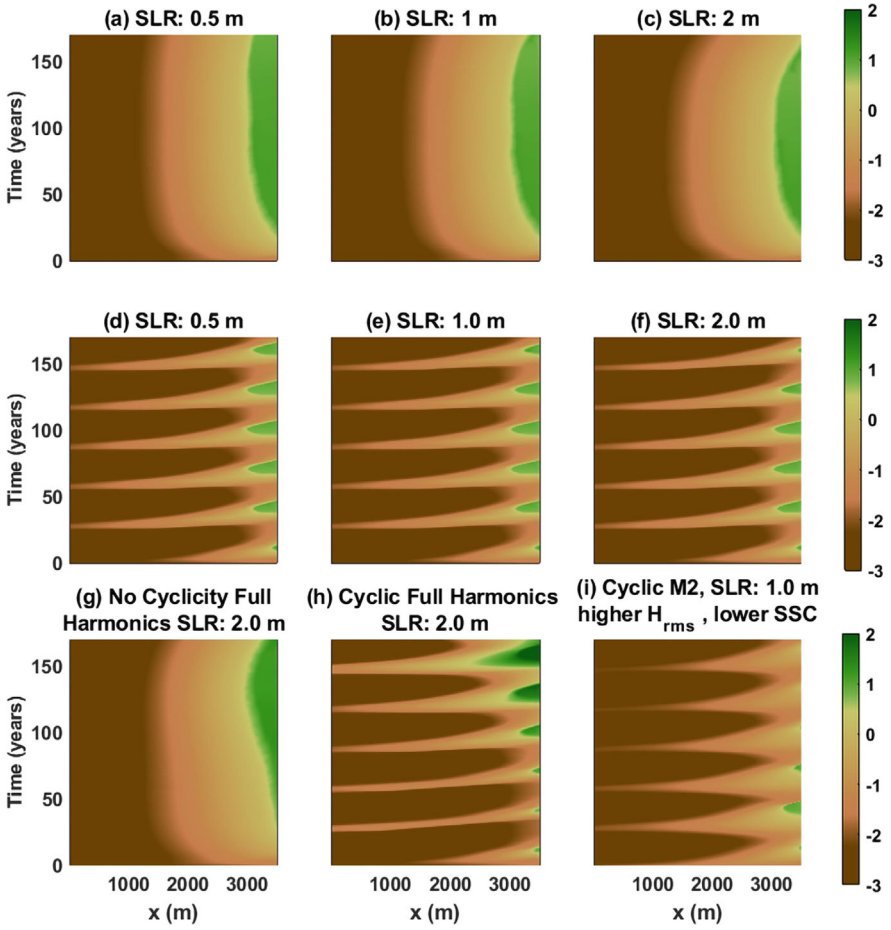

FIGURE 10 Comparison of the mangrove – mudflat evolution of the bed level (m) under SLR for the conditions under (a–c) constant tidally driven M2 conditions, (d–f) cyclic tidal-driven M2 conditions, (g) non-cyclic with astronomic forcing, (h) cyclic tidally driven astronomic forcing and (i) cyclic M2 with increased wave height (>0.55 m) and lower sediment concentration (<0.2 kg/m$^{3)}$, for 170 years. For the latter we highlight how essential the mudbank dynamics are towards the stability of the foreshore.

of the resilience of the mangrove-mudflat system under SLR with the perspective of the larger migrating mudbank dynamics along the wave-exposed Guyana coastline. However, this model does not replicate the mudbank migration itself but instead applies assumed sediment transport and wave drivers to representatively force the seaward boundary. A big challenge still lies in understanding and modelling the mudbank migration itself, but this is beyond the scope of this paper.

4.1 | Adaptation timescales and equilibrium

Our model forcing covers three characteristic timescales, i.e. tides (∼12 hours), mudbank migration (∼30 years) and sea level rise (∼century). Each of these forcing timescales is associated with a morphodynamic adaptation timescale where morphodynamic adaptation lags behind changes in forcing. Regular M2 tidal forcing leads to an equilibrium profile within 40 years. Imposing cyclically varying boundary conditions for the M2 system leads to a cyclically varying system in dynamic equilibrium within about 60 years. While tidal forcing with full harmonics develops to a state of dynamic equilibrium on much longer timespans (>100 years). SLR leads to a disturbed system with adaptation timescales longer than the current extent of the runs of 170 years. Depending on the SLR rate, Huismans et al. (2022), Lodder et al. (2019), van der Wegen et al. (2017) and Elmilady et al. (2019) suggest that SLR would bring a tidal system out of equilibrium and partially drown it by creating an "overdepth". This overdepth leads to an increase in sediment import (if available) so that after some time, the sediment import compensates for the sediment required to have the bed level follow a linear SLR. The system thus accretes and follows SLR after an initial period of drowning. The same holds true here for the modelled system with constant M2 conditions and cyclically varying M2 conditions under low rates of SLR. However, as the rate of SLR increases, the width of the mangrove platform decreases, and the system's ability to adapt reduces. The adaptation capacity of longer model runs may differ. Interestingly, systems applying full harmonics with constant and cyclically varying tidal conditions seem to have a larger adaptation capacity than the M2-only tidal forcing. This may be attributed to the higher water level conditions that are present in the full harmonics scenario, under which conditions sediment is transported more landward and can deposit at higher elevations for M2-only conditions. As such, with full harmonics, the system is more easily able to deliver the sediment required to adapt, once sediment is available.

An intriguing question relates to how the three adaptation timescales interact. Model results (see section 3.1) show that cyclicity

leads to a dynamic equilibrium with a repetitive but regular morphodynamic behaviour following the cyclic forcing conditions. However, equilibrium is not reached for the end members of the forcing conditions, that is, the conditions of maximum and minimum values for wave height, wave period and sediment concentration. The mudflat profiles during the cyclic process are never in equilibrium with their prevailing tidal forcing. The next question relates to whether such a cyclic system is more resilient to SLR than a non-cyclic system. Or, similarly, if a system under M2-only forcing is more resilient than a system under full harmonic forcing. To that end, we carried out another run forced by the M2 forcing only that leads to a mangrove belt width that is the average of the cyclically varying belt width described before. Model results (see section 3.4) show that constant M2 forcing and constant astronomic forcing produce profiles with similar elevations as their cyclically driven counterpart but have characteristically wider mangrove belts. With the full harmonic forcing, the tidal non-linearity gives way to the increased landward transport and profiles with higher elevations and wider platforms. Model results show similar patterns with smaller morphological factors, and longer runs attain equilibrium conditions. Under SLR, the systems dominated by the three forcing types are able to adapt with varying extents of intertidal losses. The loss of viable areas for mangrove growth after 100 years of SLR increases with increasing water depths for constant and cyclically driven M2 systems. However, the tidal non-linearity accompanying systems with astronomic forcing enables the recovery of the intertidal area from the 'initial drowning' even under 2.0 m of SLR. Despite the similarities in the height and width of the platform under constant and cyclic M2 forcing, the mangroves occupying the intertidal area are more mature and resilient to changing abiotic factors in the non-cyclic case. This translates to a delayed loss of intertidal area by almost 10 years in the non-cyclic system under SLR (see section 4.2).

4.2 | Tipping Point of mangrove-mudflat systems under SLR

Our modelling approach closely examines the spatial dynamics of drowning due to SLR. For the mangrove-mudflat system, resilience under SLR depends on maintaining profiles above critical water levels and ensuring positive bed level changes that match or exceed SLR rates. The system's inertia enhances its adaptive capacity as mudbank impacts slowly transfer to intertidal areas (Belliard et al., 2023). Higher SLR rates result in greater drowning of intertidal areas, with 50% of viable areas lost under a 1 m SLR scenario and 90% loss under a 2 m SLR scenario, exacerbated by regional subsidence. SLR impacts are significant under increased wave heights and sediment supply deficits (Figure 10i). Larger SLR and stronger waves lead to more landward mud distribution and greater cross-shore sediment transport. The forcing of a system with full harmonics is reflected in larger cross-shore sediment transports.

The heightened mangrove platforms are the last to drown. The organic matter accumulation is a critical factor for enhancing early mangrove resilience under SLR (Figure 9). Highly productive mangroves (with rates < 3 mm/yr.) have higher and gradually prograding platforms under minor increases in water depth. However, accretion rates are not constant and may not exceed the SLR rate overtime (Rahman, 2015; Saintilan et al., 2020). Therefore, vulnerable systems can achieve higher yearly accretion rates by external sediment supply supplements or measures aimed at retaining the mudflat elevations during the mudbank phase.

5 | CONCLUSIONS

Our bio-geomorphological 1D Mflat model is the first numerical process-based approach to reproduce the periodic erosion and accretion patterns along with a mangrove-mudflat profile in equilibrium. Mflat describes the prevailing processes governing the morphodynamics of intertidal mangrove-mudflats. These include cross-shore tidal flow, wave action, sediment transport, bed level changes, vegetation growth and decay and organic matter accumulations on a high-resolution grid. Cyclic conditions over a 30-year period were imposed, varying suspended sediment concentration, wave height and periods, achieving equilibrium profiles after 40 and 60 years for non-cyclic and cyclic systems, respectively. Through an extensive sensitivity analysis, we showed that the resilience of the mangrove-mudflat system hinges on a non-linear interaction between the astronomical tidal components, the level of cyclicity and the friction imposed along the profile. Restoration efforts that stir offshore sediment can increase deposition within mangrove fringes. Key mechanisms include wave height, period, tidal range and cross-shore sediment transport. Profiles were validated using bathymetric data from 1970 to 2020. SLR scenarios over 100 years showed varying intertidal area loss, with systems forced with full harmonics reflecting larger cross-shore transports. Higher wave heights and lower sediment concentrations increased intertidal area loss. Systems forced with full harmonics reflected larger cross-shore transports.

Mflat provides a promising, open-source tool to study intertidal flat morphodynamics across a range of process scales and time periods. In this study, the fluid mud dynamics and the longshore mudbank migration are not directly included, but the model was forced with the boundary conditions expected during the absence and presence of these extensive features. With larger datasets on the hydrodynamics and longshore transport along periodic mangrove-mudflats, it is possible that a better fit could be obtained. Optimization of the validated profile can be carried out in future research.

PERMISSION TO REPRODUCE MATERIAL FROM OTHER SOURCES

Not applicable. All figures and content have been produced by the authors.

AUTHOR CONTRIBUTIONS

This study presents a section of the doctoral research of USNB. The framework of the Mflat model without vegetation was developed by MvdW and is openly available via https://doi.org/10.1029/2019JC015492. The development and testing of the vegetation module within the Mflat framework were executed by USNB and AL under the guidance of MvdW. The model calibration and validation for the migrating mudbank coastline in Guyana were carried out by USNB and MvdW. MvdW, JR and USNB ran executables for the model simulations. The sensitivity analysis and scenario analysis for

SLR were also done by USNB under the supervision of MvdW and JR. USNB wrote the article and designed the outline of the manuscript with input from MvdW and JR. All authors reviewed, revised and approved the manuscript.

ACKNOWLEDGEMENTS

The authors gratefully acknowledge the contributions of Vasileos Ntriankos, who tested the Mflat vegetation module for mudflat development under storms. This work is openly available on the Delft University of Technology research repository via http://resolver.tudelft.nl/uuid:5bf2082a-1980-4a7a-ab81-a7b9a126fcaf. Additionally, much appreciation is extended to Johan (Han) Winterwerp and Bob Smits, with whom we worked on the Green-grey Guidelines for Guyana and whose insights enhanced our understanding of the unique dynamics of migrating mudbanks and mangrove-mudflat systems.

CONFLICT OF INTEREST STATEMENT

The authors declare that the research was conducted in the absence of any commercial or financial relationships that could be construed as a potential conflict of interest.

DATA AVAILABILITY STATEMENT

The data that support the findings of this study are openly available in Advancing Resilience Measures for Vegetated Coastline (ARM4V at https://doi.org/10.4121/c.5715269).

ORCID

Üwe S. N. Best https://orcid.org/0000-0002-7099-945X
Alexandre Legay https://orcid.org/0000-0003-2932-1820
Johan Reyns https://orcid.org/0000-0002-0849-1532
Mick van der Wegen https://orcid.org/0000-0002-5227-2679

REFERENCES

Adame, M., Reef, R., Santini, N., Najera, E., Turschwell, M., Hayes, M., et al. (2021) Mangroves in arid regions: ecology, threats, and opportunities. *Estuarine, Coastal and Shelf Science*, 248, 106796. Available from: https://doi.org/10.1016/j.ecss.2020.106796

Allison, M., Nittrouer, C. & Kineke, G. (1995) Seasonal sediment storage on mudflats adjacent to the Amazon River. *Marine Geology*, 125, 303–328.

Allison, M.A. & Lee, M.T. (2004) Sediment exchange between Amazon mudbanks and shore-fringing mangroves in French Guiana. *Marine Geology*, 208(2-4), 169–190. Available from: https://doi.org/10.1016/j.margeo.2004.04.026

Allison, M.A., Lee, M.T., Ogston, A.S. & Aller, R.C. (2000) Origin of Amazon mudbanks along the northeastern coast of South America. *Marine Geology*, 163(1-4), 241–256. Available from: https://doi.org/10.1016/S0025-3227(99)00120-6

Anthony, E.J., Gardel, A. & Gratiot, N. (2014) Fluvial sediment supply, mud banks, cheniers and the morphodynamics of the coast of South America between the Amazon and Orinoco river mouths. *Geological Society, London, Special Publications*, 388(1), 533–560. Available from: https://doi.org/10.1144/SP388.8

Anthony, E.J., Gardel, A., Gratiot, N., Proisy, C., Allison, M.A., Dolique, F., et al. (2010) The Amazon-influenced muddy coast of South America: a review of mud-bank–shoreline interactions. *Earth-Science Reviews*, 103(3-4), 99–121. Available from: https://doi.org/10.1016/j.earscirev.2010.09.008

Augusseau, P.-E., Proisy, C., Gardel, A., Brunier, G., Granjon, L., Maury, T., et al. (2025) MANG@ COAST: a spatio-temporal modeling approach of muddy shoreline mobility based on mangrove monitoring. *Environmental Modelling & Software*, 186, 106345.

Augustinus, P. (1987) The geomorphologic development of the coast of Guyana between the Corentyne River and the Essequibo River. In: *GARDINER, V. International Geomorphology*. Chichester, UK: John Wiley & Sons, pp. 1281–1292.

Augustinus, P.G. (2004) The influence of the trade winds on the coastal development of the Guianas at various scale levels: a synthesis. *Marine Geology*, 208(2-4), 145–151. Available from: https://doi.org/10.1016/j.margeo.2004.04.007

Augustinus, P.G.E.F. (1978) The changing shoreline of Suriname (South America). Doctoral Thesis, University Utrecht.

Baptist, M.J. 2005. Modelling floodplain biogeomorphology. TU Delft, Delft University of Technology.

Belliard, J.P., Gourgue, O., Govers, G., Kirwan, M.L. & Temmerman, S. (2023) Coastal wetland adaptability to sea level rise: the neglected role of semi-diurnal vs. diurnal tides. *Limnology and Oceanography Letters*, 8(2), 340–349. Available from: https://doi.org/10.1002/lol2.10298

Berger, U. & Hildenbrandt, H. (2000) A new approach to spatially explicit modelling of forest dynamics: spacing, ageing and neighbourhood competition of mangrove trees. *Ecological Modelling*, 132(3), 287–302. Available from: https://doi.org/10.1016/S0304-3800(00)00298-2

Best, U., van der Wegen, M., Reyns, J., Dijkstra, J., Roelvink, D., & van Prooijen, B. (2022a) Advancing Resilience Measures for Vegetated Coastline (ARM4VEG), Guyana. 4TU.ResearchData.Collection.

Best, Ü.S., van der Wegen, M., Dijkstra, J., Reyns, J., van Prooijen, B.C. & Roelvink, D. (2022b) Wave attenuation potential, sediment properties and mangrove growth dynamics data over Guyana's intertidal mudflats: assessing the potential of mangrove restoration works. *Earth System Science Data Discussions*, 14(5), 2445–2462.

Best, Ü.S.N. (2017) Process-based modelling of the impact of sea level rise on salt marsh & mangrove fringe-mudflat morphodynamics [An assessment of the decadal triggers for morphological evolution and restoration methods]. Master of Science (MSc.), UNESCO-IHE

Blankespoor, B., Dasgupta, S. & Lange, G.-M. (2017) Mangroves as a protection from storm surges in a changing climate. *Ambio*, 46(4), 478–491. Available from: https://doi.org/10.1007/s13280-016-0838-x

Burger, B. (2005) Wave attenuation in mangrove forests: numerical modelling of wave attenuation by implementation of a physical description of vegetation in SWAN. Masters thesis submitted to the Dep't of Civil Engineering and Geosciences, Delft University of Technology http://repository.tudelft.nl/view/ir/uuid%3A0e4c6450-fe5d-4693-9ca9-58da343448b7

Cahoon, D.R., McKee, K.L. & Morris, J.T. (2021) How plants influence resilience of salt marsh and mangrove wetlands to sea-level rise. *Estuaries and Coasts*, 44, 883–898.

Chapman, V.J. & Ronaldson, J.W. (1958) *The mangrove and saltmarsh flats of the Auckland Isthmus*. New Zealand Department of Scientific and Industrial Research Bulletin, vol. 125, 80 p.

Chen, R. & Twilley, R.R. (1998) A gap dynamic model of mangrove forest development along gradients of soil salinity and nutrient resources. *Journal of Ecology*, 86(1), 37–51. Available from: https://doi.org/10.1046/j.1365-2745.1998.00233.x

Dalrymple, O.K. & Pulwarty, R.S. (2006) Sea-level rise implications for the coast of Guyana: sea walls and muddy coasts. In: *Breaking Frontiers and Barriers in Engineering: Education, Research and Practice, Fourth LACCEI International Latin American and Caribbean Conference for Engineering and Technology (LACCET 2006) Conference Proceedings, 21–23 June*.

de Vries, J., van Maanen, B., Ruessink, G., Verweij, P. & de Jong, S. (2024) The effect of mudbank morphometrics and coastal morphology on multi-decadal coastline changes in the Guianas. *Geomorphica*, 1(1), 1–16. Available from: https://doi.org/10.59236/geomorphica.v1i1.43

de Vries, J., van Maanen, B., Ruessink, G., Verweij, P.A. & de Jong, S.M. (2022) Multi-decadal coastline dynamics in Suriname controlled by migrating subtidal mudbanks. *Earth Surface Processes and Landforms*, 47(10), 2500–2517. Available from: https://doi.org/10.1002/esp.5390

Douglas, B.C. (1995) Global sea level change: determination and interpretation. *Reviews of Geophysics*, 33(S2), 1425–1432. Available from: https://doi.org/10.1029/95RG00355

Eisma, D., Augustinus, P. & Alexander, C. (1991) Recent and subrecent changes in the dispersal of Amazon mud. *Netherlands Journal of Sea Research*, 28, 181–192.

Eisma, D. & van der Marel, H. (1971) Marine muds along the Guyana coast and their origin from the Amazon basin. *Contributions to Mineralogy and Petrology*, 31, 321–334.

Ellison, J.C. (2015) Vulnerability assessment of mangroves to climate change and sea-level rise impacts. *Wetlands Ecology and Management*, 23(2), 115–137. Available from: https://doi.org/10.1007/s11273-014-9397-8

Elmilady, H., van der Wegen, M., Roelvink, D. & Jaffe, B. (2019) Intertidal area disappears under sea level rise: 250 years of morphodynamic modeling in San Pablo Bay, California. *Journal of Geophysical Research: Earth Surface*, 124, 38–59.

Fontalvo-Herazo, M., Piou, C., Vogt, J., Saint-Paul, U. & Berger, U. (2011) Simulating harvesting scenarios towards the sustainable use of mangrove forest plantations. *Wetlands Ecology and Management*, 19(5), 397–407. Available from: https://doi.org/10.1007/s11273-011-9224-4

Friedrichs, C. (2011) *3.06-Tidal Flat Morphodynamics: A Synthesis. Treatise on Estuarine and Coastal Science*. Waltham: Academic Press, pp. 137–170.

Friess, D.A., Adame, M.F., Adams, J.B. & Lovelock, C.E. (2022) Mangrove forests under climate change in a 2 C world. *Wiley Interdisciplinary Reviews: Climate Change*, 13, e792.

Fromard, F., Puig, H., Mougin, E., Marty, G., Betoulle, J. & Cadamuro, L. (1998) Structure, above-ground biomass and dynamics of mangrove ecosystems: new data from French Guiana. *Oecologia*, 115(1-2), 39–53. Available from: https://doi.org/10.1007/s004420050489

Furukawa, K., Wolanski, E. & Mueller, H. (1997) Currents and sediment transport in mangrove forests. *Estuarine, Coastal and Shelf Science*, 44(3), 301–310. Available from: https://doi.org/10.1006/ecss.1996.0120

Gardel, A., Gensac, E., Anthony, E., Lesourd, S., Loisel, H. & Marin, D. (2011) Wave-formed mud bars: their morphodynamics and role in opportunistic mangrove colonization. *Journal of Coastal Research*, 384–387.

Gensac, E., Gardel, A., Lesourd, S. & Brutier, L. (2015) Morphodynamic evolution of an intertidal mudflat under the influence of Amazon sediment supply–Kourou mud bank, French Guiana, South America. *Estuarine, Coastal and Shelf Science*, 158, 53–62.

Hogarth, P.J. (2015) *The biology of mangroves and seagrasses*. Oxford, UK: Oxford University Press.

Horstman, E. (2014) The mangrove tangle: short-term bio-physical interactions in coastal mangroves. PhD Doctoral Thesis, University of Twente.

Horstman, E.M., Lundquist, C.J., Bryan, K.R., Bulmer, R.H., Mullarney, J.C. & Stokes, D.J. (2018) The dynamics of expanding mangroves in New Zealand. In: *Threats to mangrove forests: hazards, vulnerability, and management. Coastal Research Library*, vol. 25. Cham: Springer International Publishing, pp. 23–51. Available from: https://doi.org/10.1007/978-3-319-73016-5_2

Hu, Z., van der Wal, D., Cai, H., van Belzen, J. & Bouma, T.J. (2018) Dynamic equilibrium behaviour observed on two contrasting tidal flats from daily monitoring of bed-level changes. *Geomorphology*, 311, 114–126. Available from: https://doi.org/10.1016/j.geomorph.2018.03.025

Huismans, Y., van der Spek, A., Lodder, Q., Zijlstra, R., Elias, E. & Wang, Z.B. (2022) Development of intertidal flats in the Dutch Wadden Sea in response to a rising sea level: spatial differentiation and sensitivity to the rate of sea level rise. *Ocean & coastal management*, 216, 105969. Available from: https://doi.org/10.1016/j.ocecoaman.2021.105969

Institutional Capacity Building Activities on Guyana's Sea Defences (ICBA). (2006) In: Government of Republic of Guyana, G. S. D. (Ed.) *Guyana Sea Defenses, Bridging Programme Progress Report Block 5 Coastal Processes*.

IPCC. (2013) The 5th assessment report. New York.

Khan, M. & Sturm, M. (1995) Assessment of the vulnerability of coastal areas to sea-level rise: case study Guyana The Hague, the Netherlands Ministry of Transport, Public Works and Water Management

Kobayashi, N., Raichle, A.W. & Asano, T. (1993) Wave attenuation by vegetation. *Journal of Waterway, Port, Coastal, and Ocean Engineering*, 119, 30–48.

Lefebvre, J.P., Dolique, F. & Gratiot, N. (2004) Geomorphic evolution of a coastal mudflat under oceanic influences: an example from the dynamic shoreline of French Guiana. *Marine Geology*, 208(2-4), 191–205. Available from: https://doi.org/10.1016/j.margeo.2004.04.008

Legay, A. (2020) *Mudflat simulation: adding the vegetation influence and its dynamics to an existing Matlab model*. IHE & ESPCI internship report. Paris, France.

Lodder, Q.J., Wang, Z.B., Elias, E.P., van der Spek, A.J., de Looff, H. & Townend, I.H. (2019) Future response of the Wadden Sea tidal basins to relative sea-level rise—an aggregated modelling approach. *Water (Basel)*, 11, 2198.

Lugo, A.E. & Snedaker, S.C. (1974) The ecology of mangroves. *Annual Review of Ecology and Systematics*, 5(1), 39–64. Available from: https://doi.org/10.1146/annurev.es.05.110174.000351

Maan, D., Prooijen, B., Wang, Z. & de Vriend, H. (2015) Do intertidal flats ever reach equilibrium? *Journal of Geophysical Research-Earth Surface*, 120, 2406–2436.

Maan, D., van Prooijen, B., Zhu, Q. & Wang, Z. (2018) Morphodynamic feedback loops control stable fringing flats. *Journal of Geophysical Research: Earth Surface*, 123, 2993–3012.

Mariotti, G. & Fagherazzi, S. (2010) A numerical model for the coupled long-term evolution of salt marshes and tidal flats. *Journal of Geophysical Research: Earth Surface*, 115(F1), 2009JF001326. Available from: https://doi.org/10.1029/2009JF001326

Mariotti, G. & Fagherazzi, S. (2013) Wind waves on a mudflat: the influence of fetch and depth on bed shear stresses. *Continental Shelf Research*, 60, S99–S110. Available from: https://doi.org/10.1016/j.csr.2012.03.001

Masson-Delmotte, V., Zhai, P., Pirani, A., Connors, S.L., Péan, C., Berger, S., et al. (2021) *Climate change 2021: The Physical Science Basis. Contribution of Working Group I to the Sixth Assessment Report of the Intergovernmental Panel on Climate Change*. Cambridge, United Kingdom and New York, NY, USA: Cambridge University Press, 2391 pp. Available from: https://doi.org/10.1017/9781009157896

Mazda, Y., Magi, M., Ikeda, Y., Kurokawa, T. & Asano, T. (2006) Wave reduction in a mangrove forest dominated by *Sonneratia* sp. *Wetlands Ecology and Management*, 14, 365–378.

Mazda, Y., Wolanski, E., King, B., Sase, A., Ohtsuka, D. & Magi, M. (1997) Drag force due to vegetation in mangrove swamps. *Mangroves and Salt Marshes*, 1(3), 193–199. Available from: https://doi.org/10.1023/A:1009949411068

Mcivor, A.L., Spencer, T., Möller, I. & Spalding, M. (2012) *Storm surge reduction by mangroves*. Natural Coastal Protection Series: Report 2. Cambridge Coastal Research Unit Working Paper 41. Cambridge, United Kingdom: The Nature Conservancy and Wetlands International.

Mcivor, A.L., Spencer, T., Möller, I. & Spalding, M. (2013) *The response of mangrove soil surface elevation to sea level rise*. Natural Coastal Protection Series: Report 3. Cambridge Coastal Research Unit Working Paper 42. Cambridge, United Kingdom: The Nature Conservancy and Wetlands International.

Mckee, K.L. (2011) Biophysical controls on accretion and elevation change in Caribbean mangrove ecosystems. *Estuarine, Coastal and Shelf Science*, 91(4), 475–483. Available from: https://doi.org/10.1016/j.ecss.2010.05.001

Meade, R.H., Dunne, T., Richey, J.E., Santos, U.D.M. & Salati, E. (1985) Storage and remobilization of suspended sediment in the lower Amazon River of Brazil. *Science*, 228, 488–490.

Mendez, F.J. & Losada, I.J. (2004) An empirical model to estimate the propagation of random breaking and nonbreaking waves over vegetation fields. *Coastal Engineering*, 51(2), 103–118. Available from: https://doi.org/10.1016/j.coastaleng.2003.11.003

Milliman, J.D., Butenko, J., Barbot, J.P. & Hedberg, J. (1982) Depositional patterns of modern Orinoco/Amazon muds on the northern Venezuelan shelf. *Journal of Marine Research*, 40, 643–657.

Morris, J.T. & Sundberg, K. (2024) Responses of coastal wetlands to rising sea-level revisited: the importance of organic production. *Estuaries and Coasts*, 47, 1735–1749.

Nardin, W., Edmonds, D. & Fagherazzi, S. (2016) Influence of vegetation on spatial patterns of sediment deposition in deltaic islands during flood. *Advances in Water Resources*, 93, 236–248. Available from: https://doi.org/10.1016/j.advwatres.2016.01.001

Piou, C., Berger, U., Hildenbrandt, H. & Feller, I.C. (2008) Testing the intermediate disturbance hypothesis in species-poor systems: a simulation experiment for mangrove forests. *Journal of Vegetation Science*, 19(3), 417–424. Available from: https://doi.org/10.3170/2008-8-18384

Rahman, A. (2015) Cliff erosion of salt marshes: experimental evaluation of the effect of vegetation characteristics and sediment properties of erodibility. Master's Thesis. The Netherlands: University of Twente.

Ren, M.-E. & Shi, Y.-L. (1986) Sediment discharge of the Yellow River (China) and its effect on the sedimentation of the Bohai and the Yellow Sea. *Continental Shelf Research*, 6, 785–810.

Roberts, W., Le Hir, P. & Whitehouse, R. (2000) Investigation using simple mathematical models of the effect of tidal currents and waves on the profile shape of intertidal mudflats. *Continental Shelf Research*, 20, 1079–1097.

Roelvink, D.J. & Reniers, A.J.H.M. (2011) *A guide to modeling coastal morphology*, vol. 12. Singapore: World Scientific Publishing.

Saad, S., Husain, M.L., Yaacob, R. & Asano, T. (1999) Sediment accretion and variability of sedimentological characteristics of a tropical estuarine mangrove: Kemaman, Terengganu, Malaysia. *Mangroves and Salt Marshes*, 3(1), 51–58. Available from: https://doi.org/10.1023/A:1009936014043

Saintilan, N., Khan, N., Ashe, E., Kelleway, J., Rogers, K., Woodroffe, C.D., et al. (2020) Thresholds of mangrove survival under rapid sea level rise. *Science*, 368(6495), 1118–1121. Available from: https://doi.org/10.1126/science.aba2656

Samiksha, S., Vethamony, P., Rogers, W.E., Pednekar, P., Babu, M. & Dineshkumar, P. (2017) Wave energy dissipation due to mudbanks formed off southwest coast of India. *Estuarine, Coastal and Shelf Science*, 196, 387–398. Available from: https://doi.org/10.1016/j.ecss.2017.07.018

Shugart, H. H. (1984) A theory of forest dynamics: the ecological implications of forest succession models.

Slangen, A.B., Palmer, M.D., Camargo, C.M., Church, J.A., Edwards, T.L., Hermans, T.H., et al. (2023) The evolution of 21st century sea-level projections from IPCC AR5 to AR6 and beyond. *Cambridge Prisms: Coastal Futures*, 1, e7. Available from: https://doi.org/10.1017/cft.2022.8

Smits, B.P., Winterwerp, J.C. & Best U. (2022). Guyana Mangrove-Seawall Engineering Guidance.

Spenceley, A. (1977) The role of pneumatophores in sedimentary processes. *Marine Geology*, 24(2), M31–M37. Available from: https://doi.org/10.1016/0025-3227(77)90001-9

Swales, A., Bentley, Sr, S. J., Lovelock, C.E. (2015) Mangrove-forest evolution in a sediment-rich estuarine system: opportunists or agents of geomorphic change? *Earth Surface Processes and Landforms*, 40(12),1672–1687.

Swales, A. & Lovelock, C.E. (2020) Comparison of sediment-plate methods to measure accretion rates in an estuarine mangrove forest (New Zealand). *Estuarine, Coastal and Shelf Science*, 236, 106642.

Taylor, K.H. & Purkis, S.J. (2012) Evidence for the southward migration of mud banks in Florida Bay. *Marine Geology*, 311, 52–56.

Toorman, E.A., Anthony, E., Augustinus, P.G., Gardel, A., Gratiot, N., Homenauth, O., et al. (2018) Interaction of mangroves, coastal hydrodynamics, and morphodynamics along the coastal fringes of the Guianas. In: *Threats to mangrove forests: hazards, vulnerability, and management*. Cham: Springer International Publishing, pp. 429–473.

van der Wegen, M., Jaffe, B., Foxgrover, A. & Roelvink, D. (2017) Mudflat morphodynamics and the impact of sea level rise in South San Francisco Bay. *Estuaries and Coasts*, 40(1), 37–49. Available from: https://doi.org/10.1007/s12237-016-0129-6

van der Wegen, M., Roelvink, J. & Jaffe, B.E. (2019) Morphodynamic resilience of intertidal mudflats on a seasonal time scale. *Journal of Geophysical Research: Oceans*, 124, 8290–8308.

van Ledden, M., Vaughn, G., Lansen, J., Wiersma, F. & Amsterdam, M. (2009) Extreme wave event along the Guyana coastline in October 2005. *Continental Shelf Research*, 29(1), 352–361. Available from: https://doi.org/10.1016/j.csr.2008.03.010

van Maanen, B., Coco, G. & Bryan, K.R. (2015) On the ecogeomorphological feedbacks that control tidal channel network evolution in a sandy mangrove setting. *Proceedings of the Royal Society A: A Mathematical, Physical and Engineering Sciences*, 471(2180), 20150115. Available from: https://doi.org/10.1098/rspa.2015.0115

van Rooijen, A., McCall, R., de van Thiel Vries, J., van Dongeren, A., Reniers, A. & Roelvink, J. (2016) Modeling the effect of wave-vegetation interaction on wave setup. *Journal of Geophysical Research: Oceans*, 121, 4341–4359.

van Wesenbeeck, B.K., Wolters, G., Antolínez, J.A., Kalloe, S., Hofland, B., de Boer, W., et al. (2022) Wave attenuation through forests under extreme conditions. *Scientific Reports*, 12(1), 1884. Available from: https://doi.org/10.1038/s41598-022-05753-3

van Zelst, V., Dijkstra, J.T., van Wesenbeeck, B.K., Eilander, D., Morris, E.P., Winsemius, H.C., et al. (2021) Cutting the costs of coastal protection by integrating vegetation in flood defences. *Nature Communications*, 12, 1–11.

Vantrepotte, V., Gensac, E., Loisel, H., Gardel, A., Dessailly, D. & Mériaux, X. (2013) Satellite assessment of the coupling between in water suspended particulate matter and mud banks dynamics over the French Guiana coastal domain. *Journal of South American Earth Sciences*, 44, 25–34. Available from: https://doi.org/10.1016/j.jsames.2012.11.008

Walcker, R., Anthony, E.J., Cassou, C., Aller, R.C., Gardel, A., Proisy, C., et al. (2015) Fluctuations in the extent of mangroves driven by multidecadal changes in North Atlantic waves. *Journal of Biogeography*, 42, 2209–2219.

Welage, S.J. (2005) Coastal evolution Guyana: modelling and a historical investigation. MSc. Master Thesis. The Netherlands: TU Delft.

Wells, J.T. & Coleman, J.M. (1981) Periodic mudflat progradation, northeastern coast of South America; a hypothesis. *Journal of Sedimentary Research*, 51(4), 1069–1075. Available from: https://doi.org/10.2110/jsr.51.1069

Wells, J.T., Coleman, J.M. & Wiseman, W.J., JR. (1978) Suspension and transportation of fluid mud by solitary-like waves. In: *Conference Proceedings: 16th International Conference on Coastal Engineering*. Coastal Engineering 1978, pp. 1932–1952. Available from: https://doi.org/10.1061/9780872621909.1

Winterwerp, J.C., Borst, W.G. & de Vries, M.B. (2005) Pilot study on the erosion and rehabilitation of a mangrove mud coast. *Journal of Coastal Research*, 21(2), 223–230.

Winterwerp, J.C., Erftemeijer, P.L.A., Suryadiputra, N., van Eijk, P. & Zhang, L. (2013) Defining eco-morphodynamic requirements for rehabilitating eroding mangrove-mud coasts. *Wetlands*, 33(3), 515–526. Available from: https://doi.org/10.1007/s13157-013-0409-x

Woodroffe, C.D. (1990) The impact of sea-level rise on mangrove shorelines. *Progress in Physical Geography*, 14(4), 483–520. Available from: https://doi.org/10.1177/030913339001400404

Woodroffe, C.D., Rogers, K., McKee, K.L., Lovelock, C.E., Mendelssohn, I. & Saintilan, N. (2016) Mangrove sedimentation and response to relative sea-level rise. *Annual Review of Marine Science*, 8, 243–266. Available from: https://doi.org/10.1146/annurev-marine-122414-034025

Xie, D., Schwarz, C., Kleinhans, M.G., Bryan, K.R., Coco, G., Hunt, S., et al. (2023) Mangrove removal exacerbates estuarine infilling through landscape-scale bio-morphodynamic feedbacks. *Nature Communications*, 14(1), 7310. Available from: https://doi.org/10.1038/s41467-023-42733-1

Xie, D., Schwarz, C., Kleinhans, M.G., Zhou, Z. & van Maanen, B. (2022) Implications of coastal conditions and sea-level rise on mangrove

vulnerability: a bio-morphodynamic modeling study. *Journal of Geophysical Research: Earth Surface*, 127(3), e2021JF006301. Available from: https://doi.org/10.1029/2021JF006301

Zhang, K., Liu, H., Li, Y., Xu, H., Shen, J., Rhome, J., et al. (2012) The role of mangroves in attenuating storm surges. *Estuarine, Coastal and Shelf Science*, 102, 11–23.

SUPPORTING INFORMATION

Additional supporting information can be found online in the Supporting Information section at the end of this article.

How to cite this article: Best, Üwe S. N., Legay, A., Reyns, J. & van der Wegen, M. (2025) Morphodynamic adaptation timescales of the Guyana mangrove-mudflat system: Are coastlines shaped by migrating mudbanks more resilient against sea level rise? *Earth Surface Processes and Landforms*, 50(10), e70135. Available from: https://doi.org/10.1002/esp.70135